**PROJECT EXECUTIVE SUMMARY**

The HEAVYcOPTer project is aimed at improving the engine integration of a heavy helicopter, namely the AW101, by using advanced numerical optimization methodologies. In particular, engine intake and exhaust systems were considered as components to be optimized. The intake performance was ameliorated by reducing the total pressure losses and the inlet flow distortion at the engine interface at two relevant flight conditions, i.e. hover and forward flight. Reduction in the backpressure was instead considered as the main goal of the exhaust optimization, together with a proper balance of hot and cold flows for guaranteeing appropriate cooling of the engine bay. In addition, some further aerodynamic characteristics of the engine installation, like for instance potential tailboom heating, potential re-ingestion of hot gases in ground idle conditions, and effect of rotor inflow in some representative flight conditions were taken into account. To this purpose, an in-house multi-objective evolutionary algorithm was used coupled with both commercial and open-source CFD solvers. The final results confirmed the achievements of substantial improvements in engine installation performance.

**PROJECT CONTEXT AND OBJECTIVES**

The HEAVYcOPTer project is a Call for Proposal (CfP) in the framework of the CleanSky JTI, which in turn is the most ambitious aeronautical research program ever launched in Europe, essentially devoted to the identification and implementation of some breakthrough technologies aimed at improving the environmental friendliness of both fixed-wing and rotary-wing aircrafts, both in terms of noise emissions and fuel consumption.

In the Clean Sky (CS) framework, a dedicated section is devoted to rotorcraft (both helicopters and tilt-rotors), which is called Green RotorCraft (GRC). The GRC is organized in six tasks: specifically, GRC2 regards the design optimization and active flow control of both airframe and non-lifting dynamic systems for drag reduction.

The HEAVYcOPTer project refers to CS GRC2 and is aimed at implementing and applying an innovative design methodology to be used for efficient optimization targeted to engine installation improvement in a heavy helicopter, namely the AW101. To this purpose, an in-house multi-objective evolutionary algorithm coupled with commercial CFD solvers was used. In particular, effective aerodynamic design of intake and exhaust is essential for engine installation optimization and requires the accomplishment of multiple, and often conflicting, objectives in presence of multiple and multi-criteria constraints.

In the present case, the intake geometry was to be designed for maximum pressure recovery while minimizing the total pressure losses and flow distortions at Aerodynamic Interface Plane (AIP) with the engine. Several constraints were to be accounted for, i.e. the overall size and dimensions of the engine, minimum thickness issues related to construction, size and shape of the by-pass duct for particle separation, etc.

Regarding the exhaust, a shape optimization was carried out on the discharge duct with regard to its isentropic efficiency and swirl removal effectiveness by taking into account the dimensional constraints dictated by the engine exhaust. Moreover, an additional objective consisted in minimizing engine backpressure, since this is fundamental for maintaining the engine performance at the required optimum level. In addition, hot and cold fluxes were properly balanced with the aim of guaranteeing a sufficient engine bay cooling. Finally, prevention of tail boom heating, as well as avoidance of hot gas re-ingestion in sideward wind conditions were taken into account as functional constraints.

The **objectives** of the project were:

i) to set up a comprehensive and fully automatic optimal design tool, integrating the software suitable for engine installation analysis and an in-house multi-objective optimization algorithm already developed by the University of Padova;

ii) to apply such tool for the efficiency improvement of engine installation components based on the boundary conditions given by the manufacturer, in order to achieve a significant reduction in the engine installation losses.

The above mentioned objectives were achieved by means of a dedicated programming and simulation activity, where the software tools available at the leading industry premises for the design and analysis of engine installation performance will be interfaced together and with the optimization tool proposed by the UNIPD-HIT09-MDA Consortium. The result was a robust procedure where only the initial geometry importation and parameterization were carried out off-line, while meshing, geometrical/grid manipulation, as well as CFD analyses will form an automatic loop. The optimization tool, which is capable of efficiently handling complex multi-objective problems, was applied to review the basic intake and exhaust design, with the aim of minimizing any detrimental effects on both drag and engine installation, through both a reliable intake and exhaust shaping and an analysis and control of flow distortion, total pressure losses and flow separation. Finally, the optimized engine installation geometry was checked for compliance with feasibility constraints in order to accomplish industrial needs for prototyping and testing.

**MAIN S&T RESULTS/FOREGROUNDS**

**Preliminary characterization of the baseline engine installation.**

The first part of the project was devoted to the setup and validation of numerical models for the air intakes and exhaust of the AW101 heavy-class helicopter to be used as a reference for the subsequent optimization phase. As it is well-known, the task of a helicopter's intake is to convey the air mass flow required by the engine with as little total pressure losses as possible to ensure high shaft power. Depending on the flight Mach number, this requires either acceleration or deceleration of the air surrounding the intake in order to match the engine flow condition demands. In addition, the flow entering the engine should be as uniform as possible to ensure stable engine operation at all flight conditions within the flight envelope of the helicopter. Typical flow non-uniformities are total pressure, swirl and total temperature distortions [1]. In compact S-shaped intakes, such as those mounted on the AW101 helicopter, the first two are quite common and connected with each other: flow separations will possibly lead to flow angularity because of the high curvature of the wall, according to the same mechanisms that produce rotating flows in pipe bends. The flow can then enter the compressor in rotation or counter-rotation direction, i.e. either decreasing or increasing the flow incidence angle relative to the compressor blades. This phenomenon can ultimately produce surge or non-recoverable rotating stall [2]. In the low subsonic regime, total pressure losses can be limited through the overall geometrical shaping and positioning of the air intake using well-established design techniques and practical guidelines [3]. The non-uniformities problem, on the other hand, is significantly more difficult to tackle; although experience exists on the distortion behavior of different types of intakes for various helicopter's projects, even today the intake-engine compatibility of a model cannot be predicted in a reliable way at the beginning of the design cycles [4]. This is mainly due to the fact that the selection of an intake type, its position on the fuselage, cross-section variation profile and longitudinal shape are not only defined by flow physics arguments.

AW101 helicopter has 3 air intakes, two at the left side of the pilot (one more lateral and one near to the engine cowling top surface) and one at the right (Figure 1 and Figure 2): only intake#1 and intake#2 (left hand side and central ones respectively) were considered in the project, since intake#3 is symmetrical to intake#1. Validation of the numerical model of air intakes was carried out against experimental results coming from a wind tunnel campaign on a 2/9th helicopter scaled model performed at AgustaWestland Ltd. Specifically, total pressure distributions at the Aerodynamic Interface Plane (AIP) were available as well as static pressure distributions over intake#2 at various flight conditions.

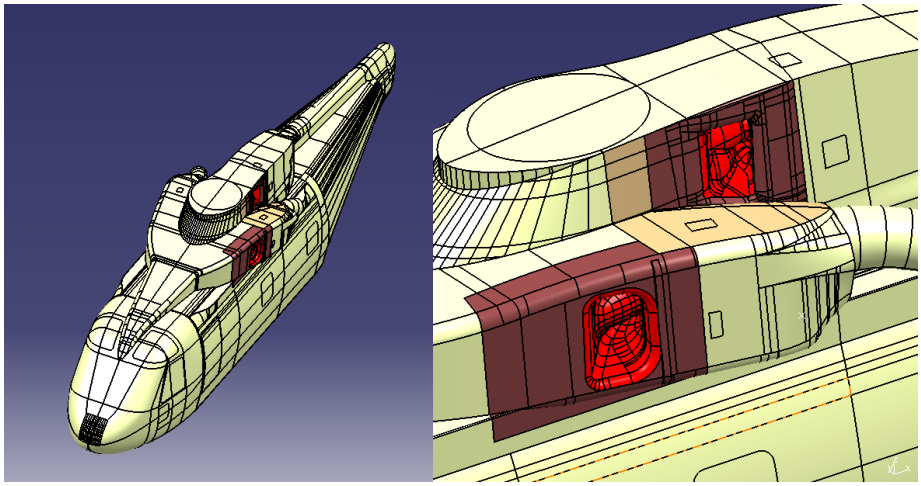

**Figure 1: AW101 Helicopter engine intake#1 and #2.**

Overall agreement between experimental and numerical results was good based mainly on DC60 profiles and total-pressure distributions evaluation (Figure 4). The correlation was more than good on wide angular sectors of the AIP plane, being less satisfactory on other narrow zones for some operating conditions, especially for intake#2 (Figure 5). Average percentage difference for the peak distortion magnitude between experimental and numerical results was around 9.6%, with the exception of the hovering case, for which a poorer agreement was registered even using more refined computational grids. Regarding static pressure prediction, correlation with experimental data was very good in capturing both the experimental trend and absolute values (Figure 3). Differences in predicted intake efficiency with respect to the experimental values were negligible (0.3% maximum deviation from experimental results). With the intakes' CFD model fully developed and validated, the full scale aerodynamic characterization was carried out in a couple of typical operative flight conditions provided by AgustaWestland Ltd, in particular one in hovering and another one in forward flight. Such activity was focused on the aerodynamic performance of the air intakes at operative conditions similar to those utilized for subsequent optimization. As a consequence, the weaknesses and the major sources of losses occurring in the baseline geometry were identified: in fact, this was fundamental to find out a proper geometry parameterization to be used for optimization in order to achieve a significant performance improvement.

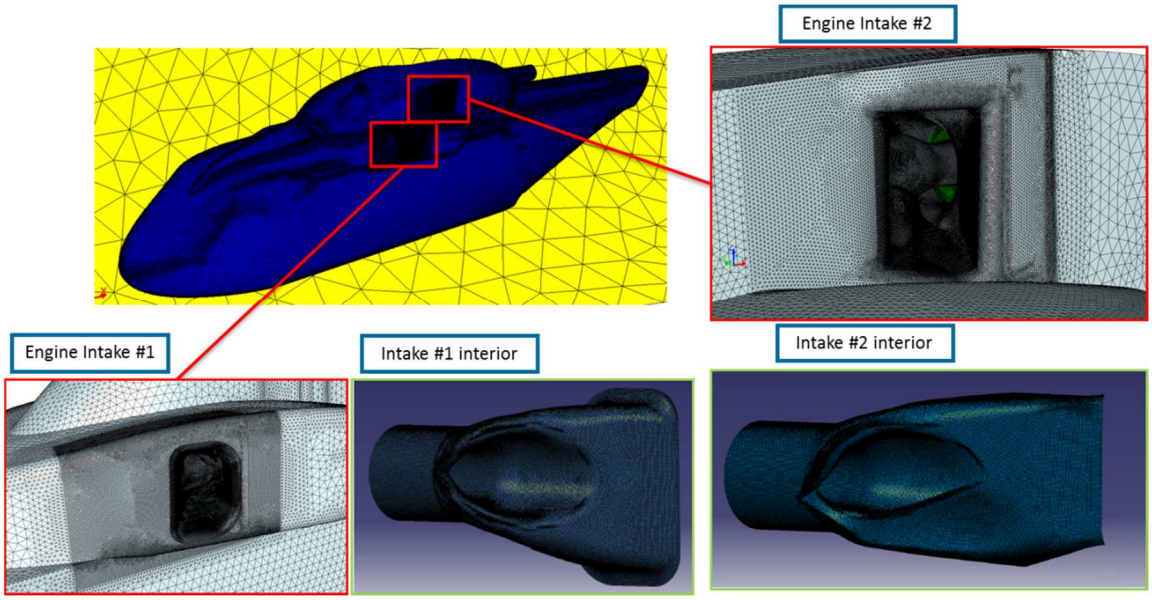


**Figure 2: Computational mesh used for validation of intakes numerical models.**

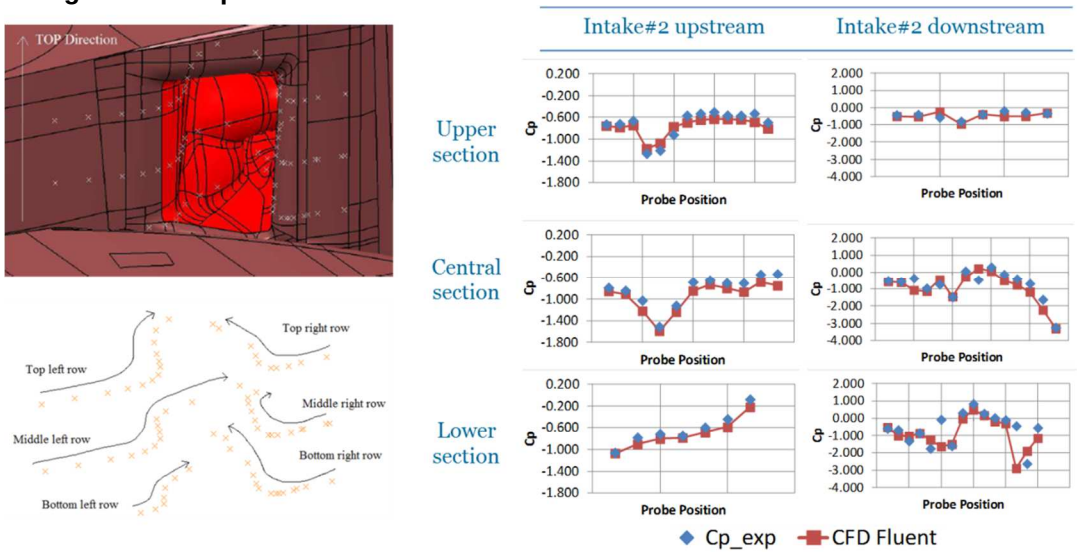


**Figure 3: Validation of the numerical model against wind tunnel data: static pressure coefficient distribution over intake#2.**

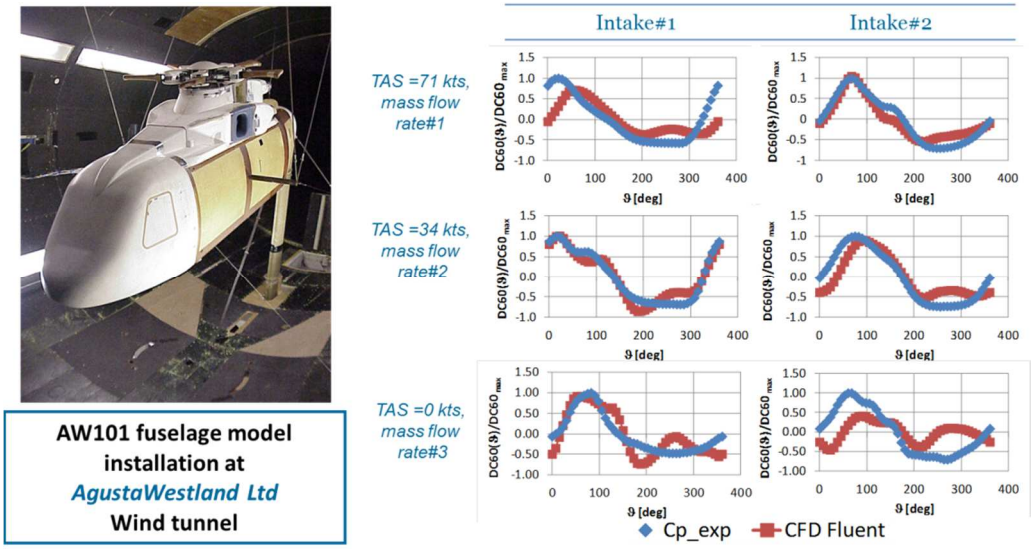


**Figure 4: Validation of the numerical model against wind tunnel data: DC60 profiles over AIP of both intake#1 and intake#2 at various flight conditions.**

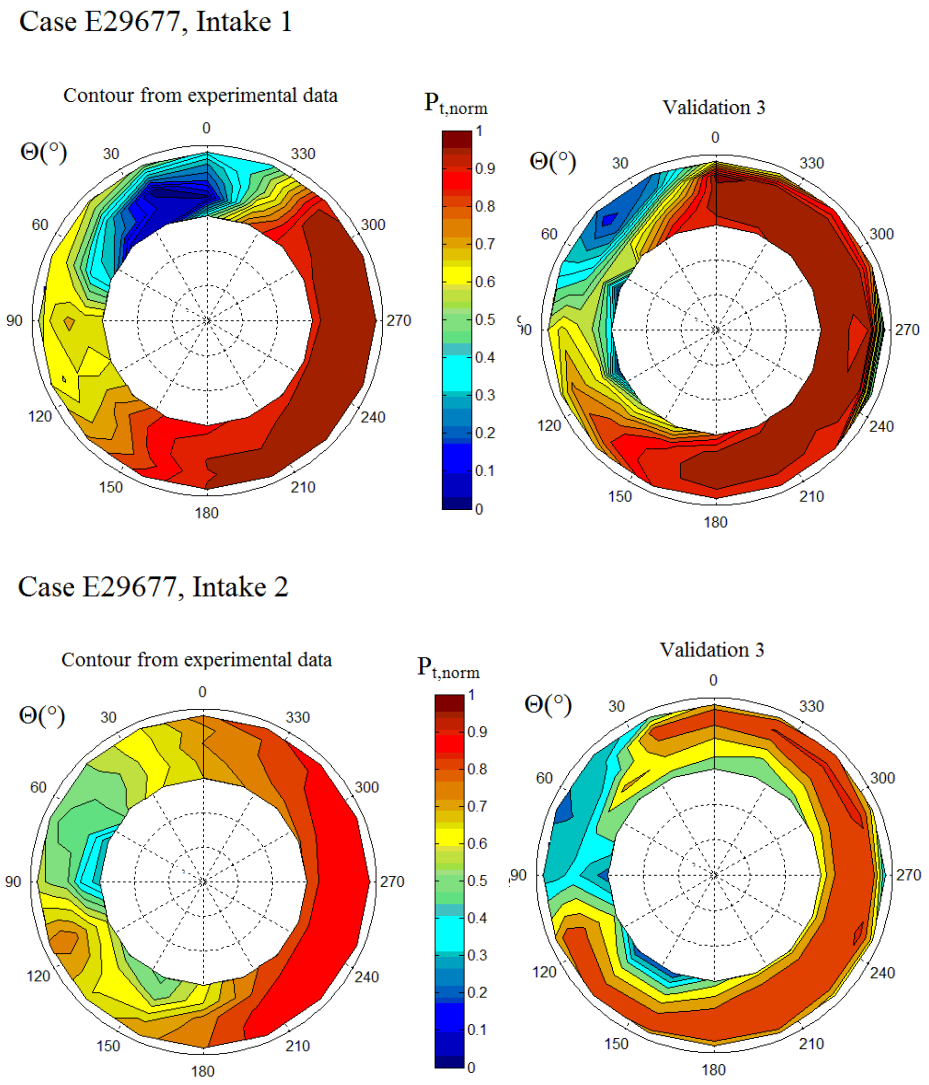


**Figure 5: : Comparison of numerical (on the right) normalised total pressure contours at the AIP with the corresponding experimental data (on the left).**

Regarding the engine exhaust, data coming from a test rig configuration which was tested at the AgustaWestland Ltd wind tunnel facility in 2004 was used for validation. Objectives of the tests were to get cold flow data on current AW101 exhaust/eductor system and to explore specific design features including fluted core nozzles for improving educted flow with minimum backpressure in order to meet AW101 performance and bay cooling requirements. These objectives were achieved through an experimental campaign on a ½ scale cold flow test rig representing the AW101 engine bay and exhaust (Figure 6). Bay inlet scoops were replaced with bell mouth entry flow gauges and a number of inlet area restrictors to replicate scoops with given loss characteristics. It is worth noting that the fluted nozzle used as the datum design was a development nozzle and not the one used on AW101. The engine rear end consisted of a swirl inducer in a scaled power turbine exit annulus. Pitot static probes were fitted to traverse across the core nozzle exit plane. Several combinations of main nozzle/exhaust pipe/swirl angle/central body were tested during the rig experimental campaign. Specifically, for validation purposes, the CFD model was set-up (Figure 7) and exhaust back pressure and entrainment ratio were calculated for two geometrical configurations of the daisy nozzle and at various exhaust mass flow rates. A thorough analysis was carried out in order to identify the proper CFD model set-up and the model was validated against experimental data. Regarding the exhaust back pressure, simulations results were demonstrated to capture the experimental trend in a satisfactory way for both the considered nozzle geometries, with a maximum percentage error of around 10%, registered at the highest analysed mass flow rate (Figure 8). Also the entrainment ratio was satisfactorily reproduced: the general trend with mass flow rate was well captured with a maximum error of ~10% with respect to experiment. In addition, the set-up of a proper swirl model to be included in the CFD simulations for reducing the mesh size and make the model more representative of the real exhaust installation was carried out. Actually, direct modelling of swirl generators is not appropriate for numerical analysis of the exhaust flight configuration and then for optimisation. In fact, this component increases the model complexity (more than two millions of volumes elements are required to model the swirl generator) while not allowing for a proper evaluation of the engine back pressure. The swirl generator induces its own amount of back pressure which is in fact not present on the real installation, since the swirl is a characteristic of the engine. To this purpose, a lumped fan model approach with radial specification of tangential velocity distribution was used to introduce a swirling component within the main flow stream. Then, the exhaust numerical model was scaled up to the full scale dimensions (including the engine bay) and a series of simulations with hot fluxes were carried out on the baseline configuration in two selected flight conditions for optimization, i.e. cruise forward flight and ground idle.

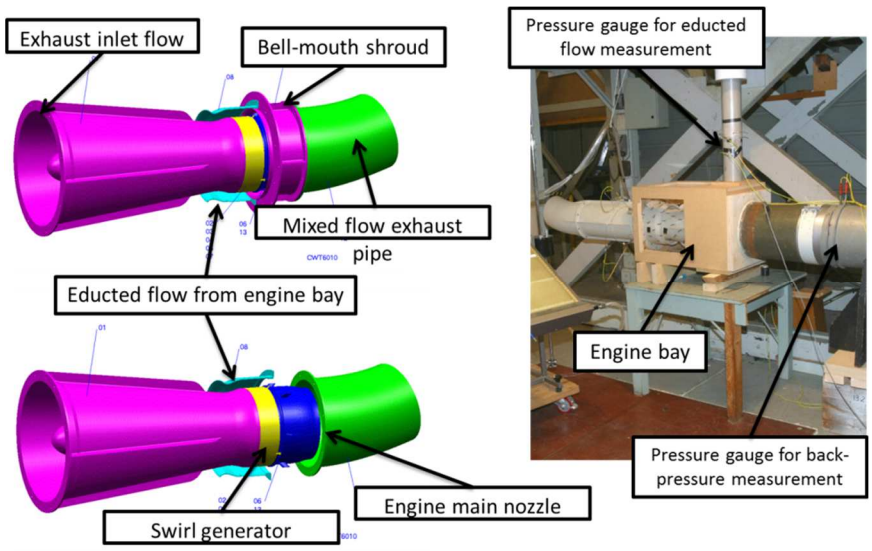


**Figure 6: Experimental test rig for the AW101 exhaust tests.**

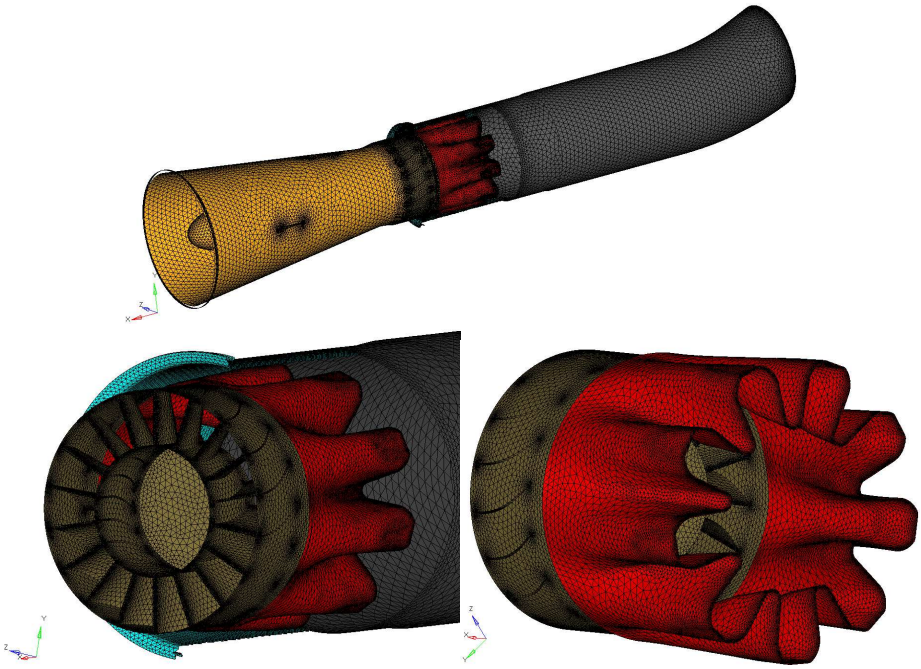

**Figure 7: Details of the computational mesh used for validation of the AW101 exhaust numerical model.**

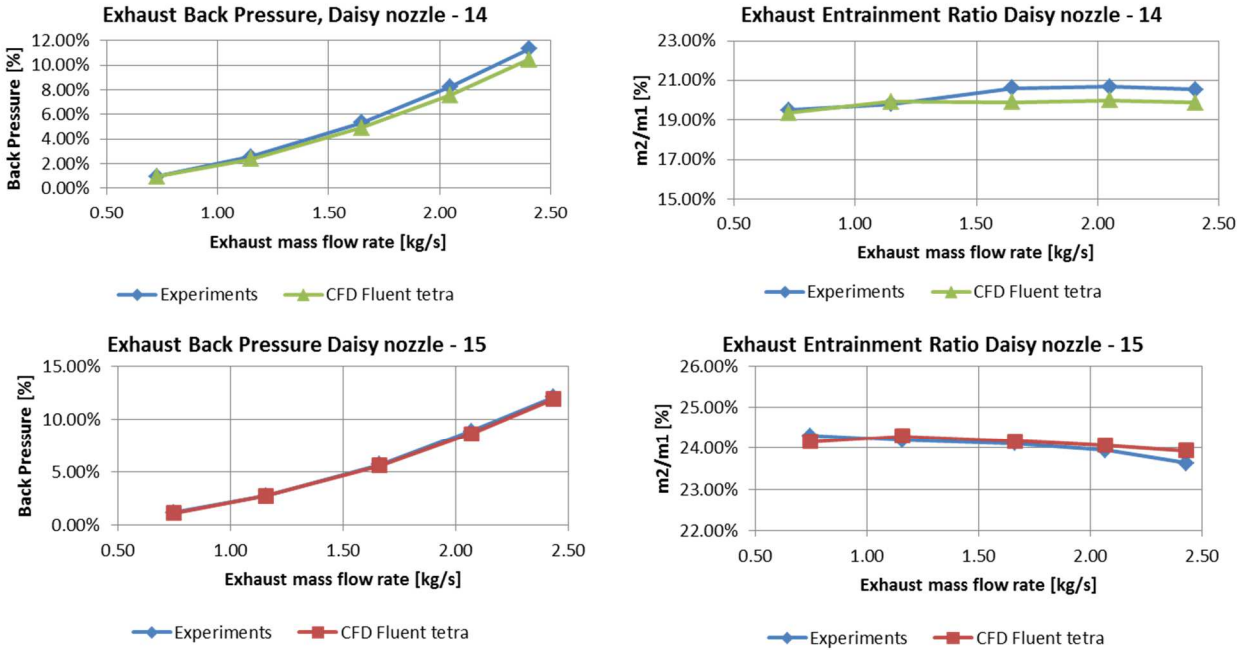


**Figure 8: Exhaust validation results: numerical backpressure and entrainment ratio against experimental data for two types of nozzles.**

With the baseline geometry fully tested and validated, the optimization problem could be formulated.

**Brief description of the optimization methodology.** The aerodynamic optimization procedure which was implemented for the HEAVYcOPTer project is structured in three phases (Figure 9):

1) Baseline model preparation and simulation phase;

2) Automatic optimization phase;

3) Post-processing and optimized CAD model reconstruction phase.

The starting point usually consists in the CAD model of the baseline configuration. In the "baseline simulation block", the current configuration of the component under consideration must be analyzed via CFD computation in the most relevant operating conditions. The assessment of the baseline solution makes it possible to gain a deeper insight into the flow field characteristics of the object under analysis; moreover, it gives fundamental indications for a proper formulation of both optimization objectives and constraints and allows to properly set up the geometrical parametric model.

When the preliminary operations have been completed, the automatic optimization can be carried out. The optimization loop is made up of three components:

1) GeDEA (Genetic Diversity Evolutionary Algorithm): advanced multi-objective optimization algorithm developed at the University of Padova ([5]), which is the selected optimization engine;

2) Altair HyperMorph®: it converts the design parameters coming out from GeDEA into morphed CFD cases, suitable for the objective function evaluation;

3) Ansys Fluent®: the selected flow solver; it takes in input the morphed CFD cases coming from HyperMorph® and gives back to GeDEA the correspondent values of the selected objective functions.

During the optimization process, GeDEA let a population of individuals (each of which corresponds to a different set of design variables and so to a different geometry configuration) "evolve" until the convergence to the Pareto optimal frontier has been reached.

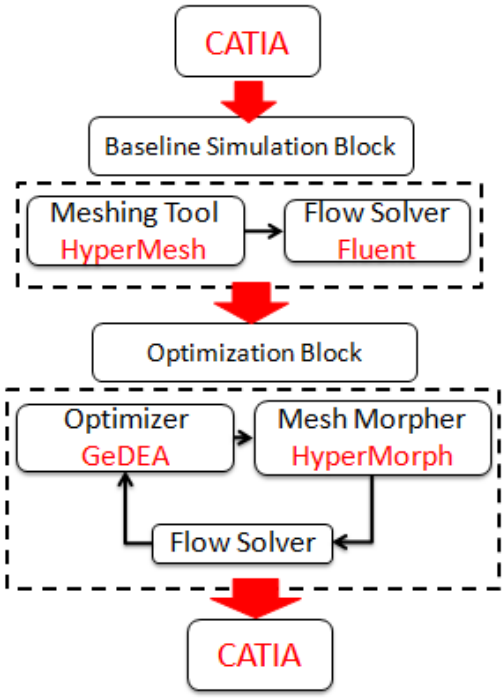


**Figure 9: Optimization method flow-chart.**

The Pareto frontier coming out from the automatic optimization loop represents a multiple set of solutions equally optimal according to the Pareto concept but of course different form the aerodynamic and

engineering point of view. In fact, each solution over the Pareto frontier may feature advantages and drawbacks with respect the other solutions. In order to choose the most appropriate solution among the optimal set a post-processing work is necessary. Thanks to the intrinsic multi-objective approach, the designer is allowed to select the solution which is more suitable for his needs, for instance choosing to privilege the improvement of one objective with respect to the other or even including other considerations such as non-aerodynamic requirements. The strength of the selected approach is that the designer can select the proper trade-off between the objectives when the optimization work has been completed and he is not forced to introduce his arbitrariness in the problem set up, as commonly happens using traditional optimization approaches.

**Engine installation optimization**

For the sake of clarity, the presentation of results has been split in two parts, regarding intakes#1 and #2 and exhaust#2, respectively. Afterwards, the main achievements regarding the overall engine integration are presented.

**Intakes Optimization.** AW101 engine intakes ducts are S-shaped ducts connecting the side entry section with the engine compressor face, commonly referred to as *Aerodynamic Interface Plane* (AIP). Layouts of AW101 engine#1 and engine#2 bay internal components were provided by AgustaWestland Ltd in order to allow the definition of geometrical modifications of the duct surfaces so as to be compliant with the installation architectural constraints (Figure 10).

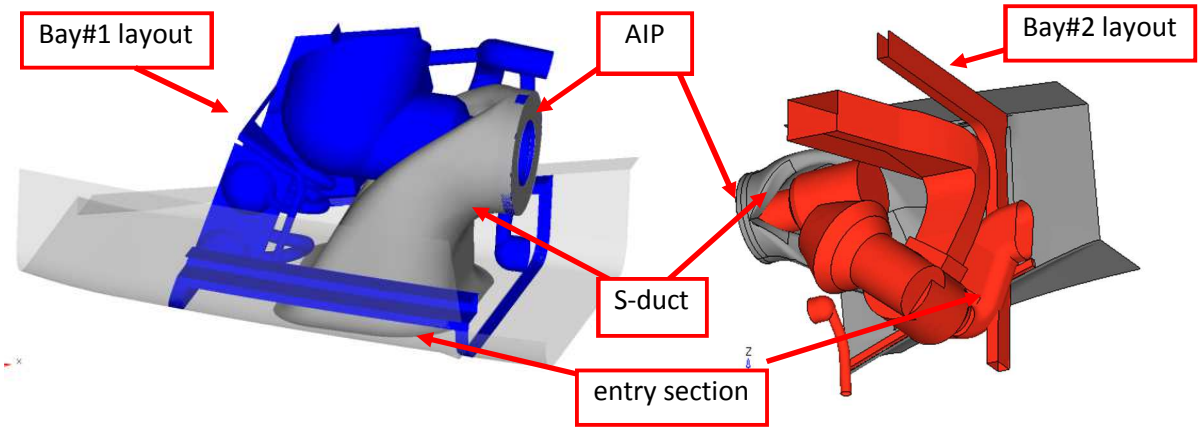


**Figure 10: Internal view of intake S-duct and bay internal components layout for engine#1 and engine#2.**

Once the main geometrical features characterizing the baseline designs were identified, design parameters were generated for the complete geometrical control of the intake#1 and intake #2 duct shapes. The morphed geometry results therefore from the linear combination of the user defined shapes multiplied by their own scaling factors:

$$\boldsymbol{v} = \sum_{i=1}^{n} \alpha_i Sh_i \qquad (1)$$

where:

- $v$ is the global displacement vector;
- $Sh_i$ are the i$^{th}$ basic shapes defined within HyperMorph®.
- $\alpha_i$ is the i$^{th}$ shape scaling factor generated by GeDEA.
- $n$ is the number of parameters for the current application.

During the automatic optimisation process, the scaling factor $\alpha_i$ represent the set of design parameters controlled by the optimization algorithm.
The shapes implemented for intake#1 and intake#2 are shown in Figure 11 and Figure 12 respectively.

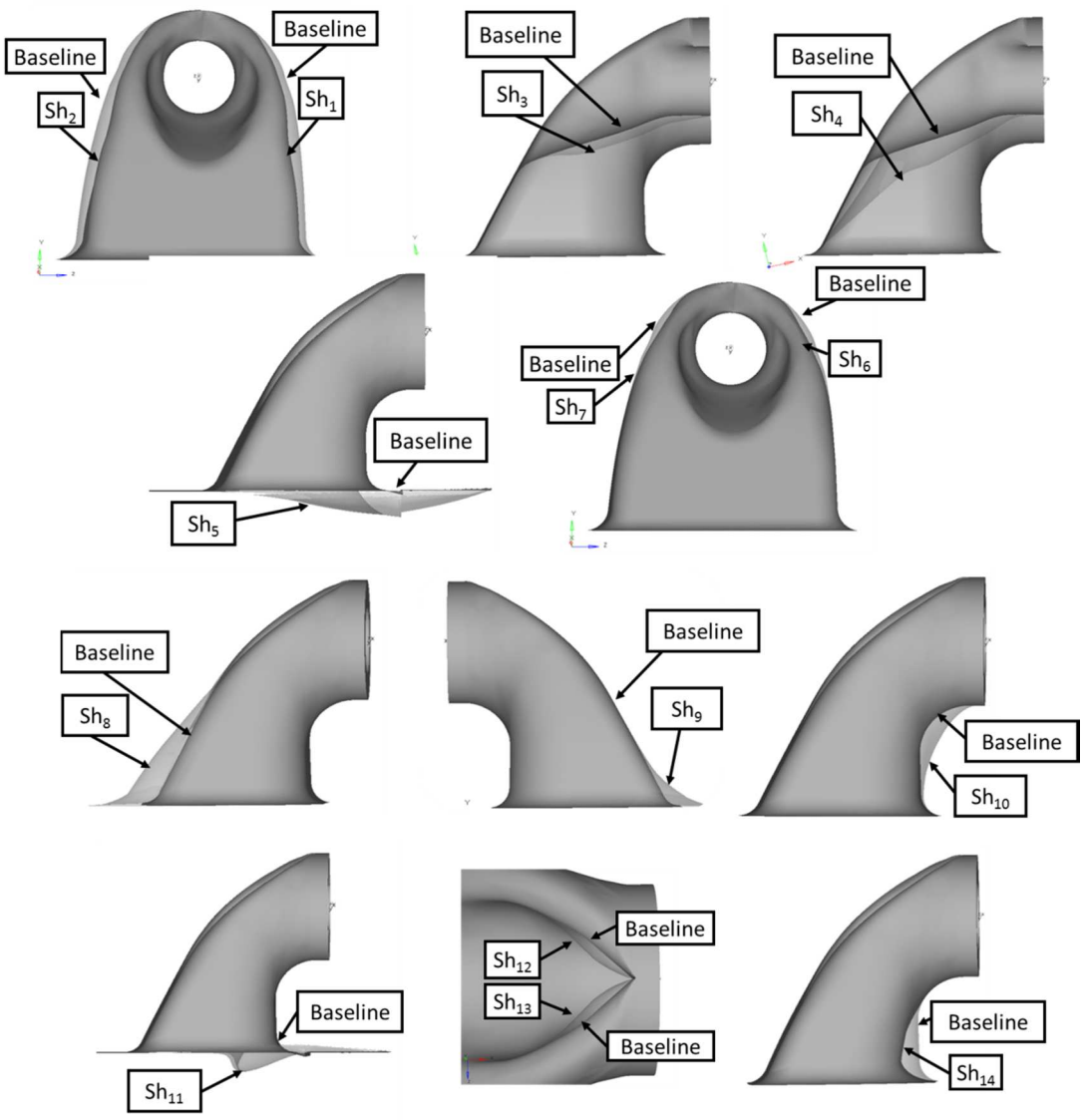


**Figure 11: Implemented shapes application on intake#1.**

A proper objective function was implemented to carry out the air intakes optimization: specifically, a bi-objective and two component vector function obtained by the sum of the total pressure loss term and a *penalty function* term was selected. It can be mathematically expressed as:

$$\text{minimize}\left\{G(x) = \left[F(x) + PF(x)\right]\right\} \tag{2}$$

where *F(x)* accounts for aerodynamic total pressure loss ($\Delta P_T$) within the intakes at the two reference flight conditions selected for optimization:

$$F(x)=\begin{bmatrix}\Delta P_T(x)\,|\,@\,hover\\ \Delta P_T(x)\,|\,@\,cruise\end{bmatrix} \tag{3}$$

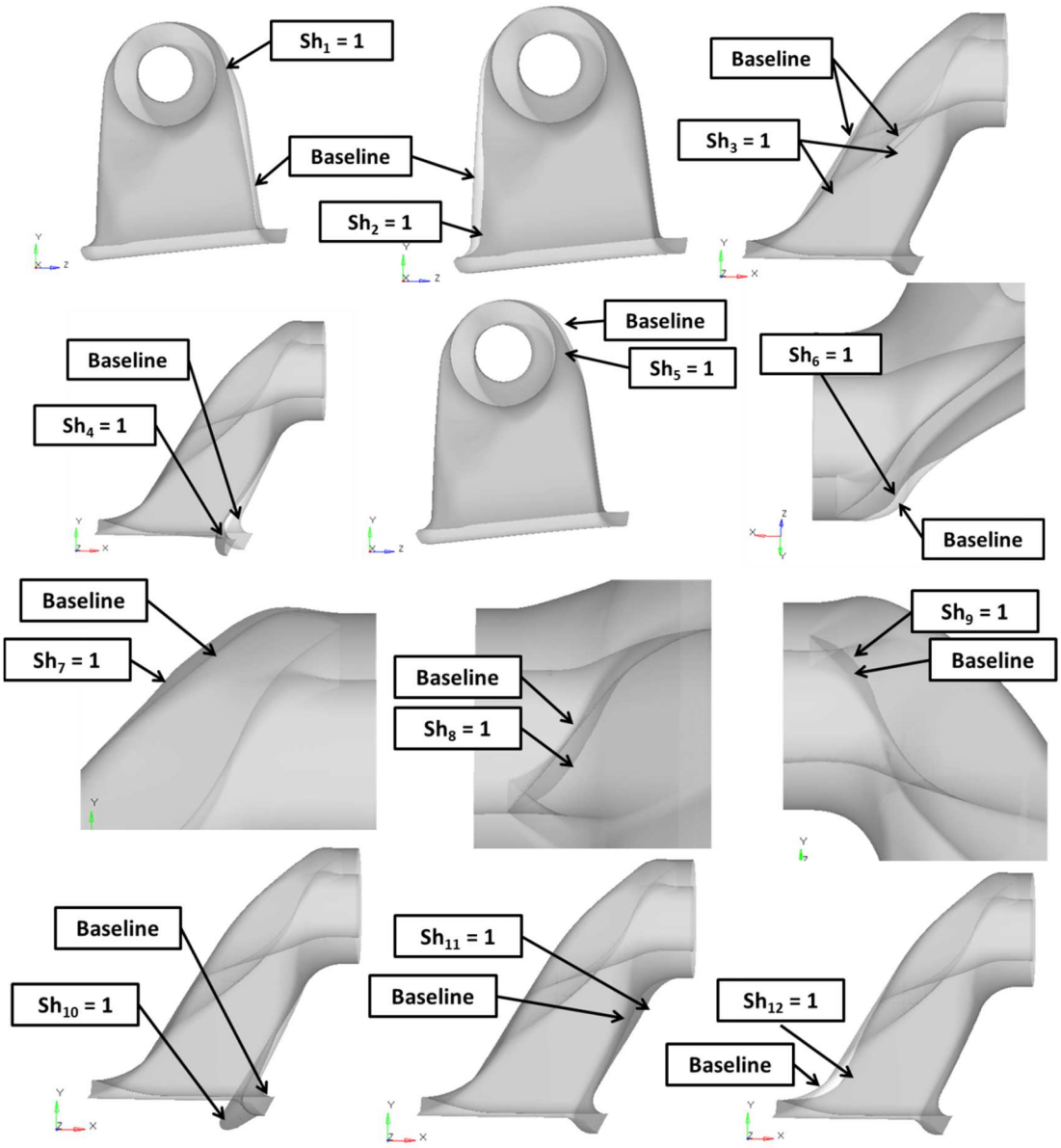


**Figure 12: Implemented shapes application on intake#2.**

The penalty function *PF(x)* introduces a functional constraint on the flow distortions at the engine inlet by worsening the score of a generic configuration with an additional term proportional to the DC60 factor difference with respect to the baseline configuration:

$$PF(x)=\begin{bmatrix}0 & \text{if } DC60(x)\le DC60_{baseline}\\ \beta\left|\dfrac{DC60(x)-DC60_{baseline}}{DC60_{baseline}}\right|^{\gamma} & \text{if } DC60(x)>DC60_{baseline}\end{bmatrix} \tag{4}$$

where the coefficients β and γ control the intensity and shape of the penalty function respectively. Again, this term was evaluated at the two flight conditions selected for optimization.

The design variables vector, ***x***, was given by the set of scaling factors, subject to the specific variable bounds of Intake#1 and Intake#2:

$$x = [\alpha_1 ..... \alpha_n] \tag{5}$$

Before the optimisation, a Design Of Experiments study was carried out for each of the air intakes in order to help in the selection of the final set of parameters to be used in the optimization. In addition, this was also helpful to provide the genetic algorithm with a suitable starting population. The automatic optimization was then run for a proper number of generations, i.e. seven for intake#1 and five for intake#2 respectively. The results were monitored, generation by generation, in terms of total pressure loss and DC60 distortion factor at both the hovering and cruise flight conditions selected for optimization. The best configuration for each air intake was finally selected among the solutions on the final Pareto front, based on the best compromise between the performance at the two selected operative conditions.
Remarkable improvement on the objective functions were achieved at the end of optimization.

Figure 13 shows the final Pareto frontier of optimized geometries (red triangles) calculated by the GeDEA algorithm for intake#1 in the objective function space, i.e. in the plane where the objectives of the optimization are given. As mentioned before, these were the minimization of the total pressure losses in hover (in abscissas) and forward flight (in ordinates). In the same figure, the performance of the initial configuration (i.e. the baseline intake to be optimized) is evidenced (blue point): as apparent, despite the number of generations was relatively small, significant improvements in both hover and cruise objective functions were achieved with respect to the baseline. The selected intake#1 optimal design was characterized by hover total pressure loss reduction of 25% with respect to the original design, while the cruise total pressure loss experienced a significant 33% reduction. For this design, the distortion level was compliant with the functional constraint in Eq. (4) in cruise, since a 37% reduction of the DC60 index was observed. The geometry comparison of the best compromise optimised design and the baseline design is illustrated in Figure 14. It is apparent that the optimised geometry is wider than the baseline in the cross sectional direction, thus improving the pressure recovery in the hover condition. On the other hand, the shaping of the rear-lip causes an increase of the stagnation pressure on the rear wall region at cruise condition; this effect in turn increases the energy available for the flow to go around the duct S-bend, improving the intake pressure recovery capabilities. At the same time, the curvature of both the front and rear wall results to be smoother with respect to the original design, reducing the severity of the S-bend. The above mentioned geometry modifications produce more uniform total pressure distributions (especially in cruise) with a lower level of distortion, as apparent from the AIP total pressure contours and total pressure losses along the intake duct illustrated in Figure 15 for both hover and forward flight. This results, together with the higher average AIP total pressure value, are expected to improve the engine performance in terms of both efficiency and stability.

Regarding intake#2, the final Pareto frontier is shown in Figure 16, which is also helpful in assessing the contribution of the flow distortion, taken into account by means of the penalty factor (4), to the fitness score of the final Pareto frontier. As this term is excluded, the scores, now representative of the total pressure loss reduction only at both flight conditions, move in the plane of the objective function. Whilst at cruise all Pareto individuals exhibit a reduction in the DC60 factor, this is not verified at hovering. As a consequence, the no-penalty frontier moves to the left in the graph, with an average displacement of 10%. The selected intake#2 optimal solution features the best compromise in the overall performance of the air intake#2: in fact, the total pressure loss reduction at cruise condition is very close to the maximum margin (-25%) and the distortion level is compliant with the functional constraint (a -28% reduction of the DC60

index was observed). At the same time, total pressure recovery capabilities at hover are worsened to a limited extent since the total pressure loss increase is +11%. Figure 17 shows the geometry comparison

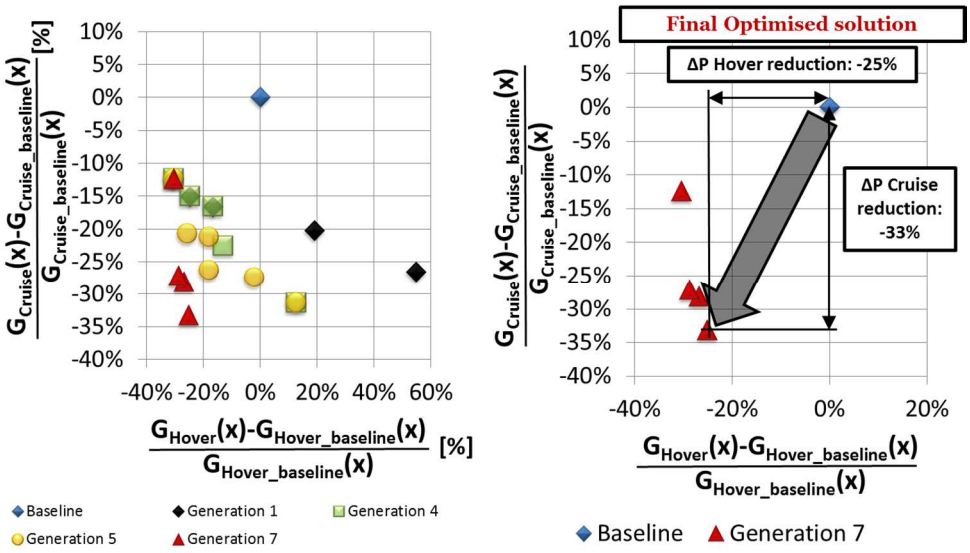


**Figure 13: Evolution of the Pareto front for optimization of intake#1.**

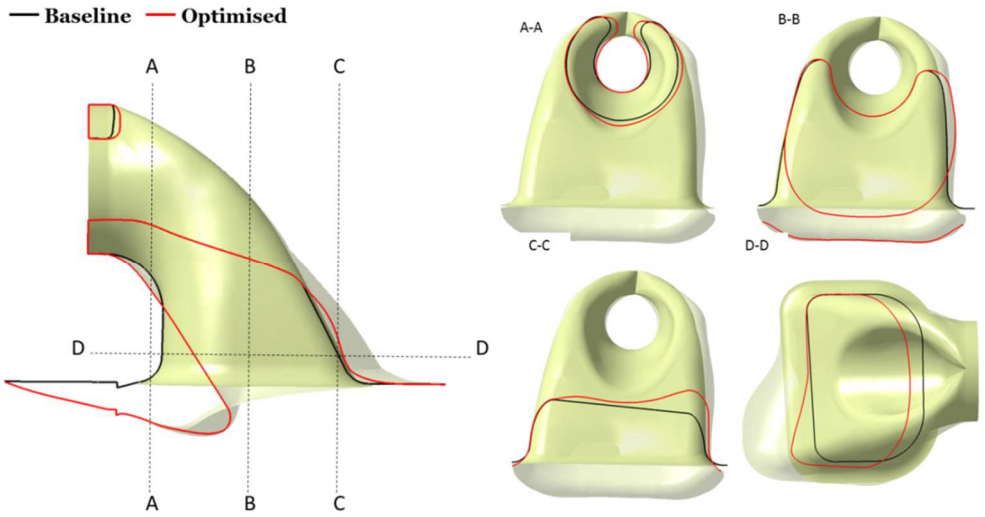


**Figure 14: Optimised shape of intake#1 compared to the baseline.**

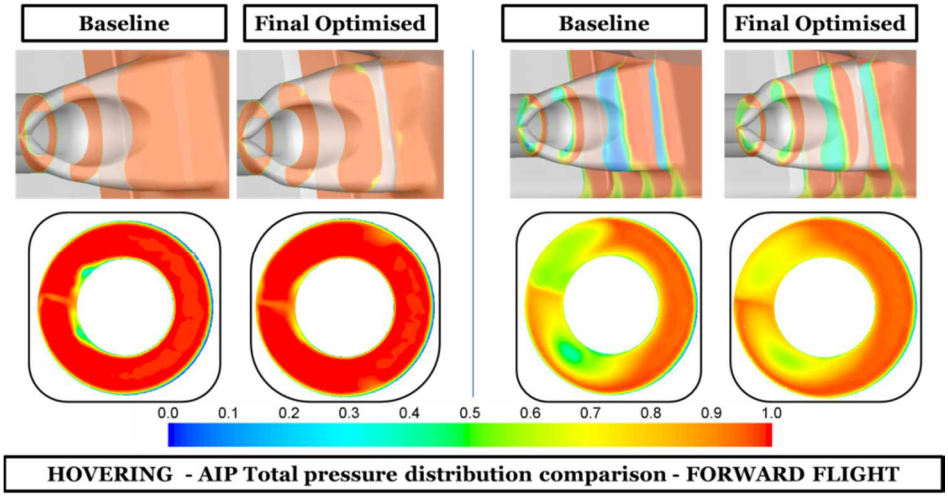


**Figure 15: Optimisation results on intake#1: total pressure losses along the optimised intake duct and over the AIP vs. baseline in hover (on the left) and cruise condition (on the right).**

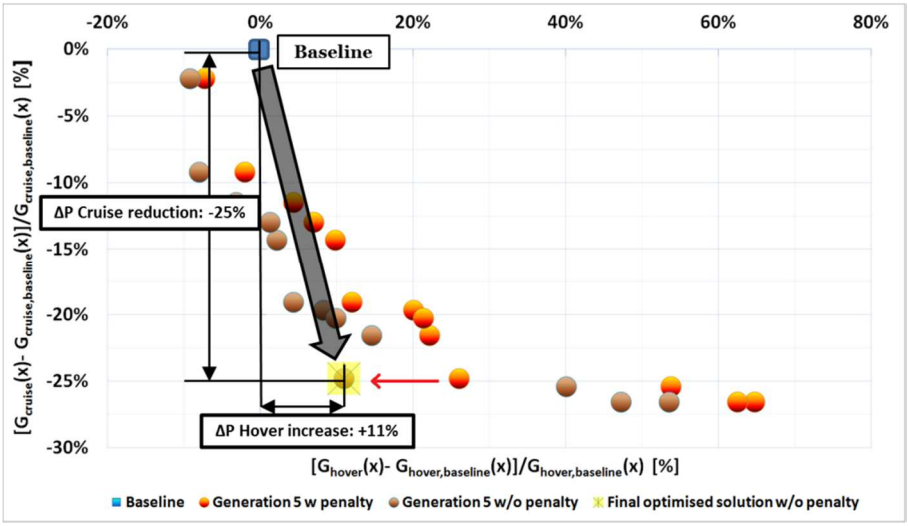


**Figure 16: Evolution of the Pareto front for optimization of intake#2.**

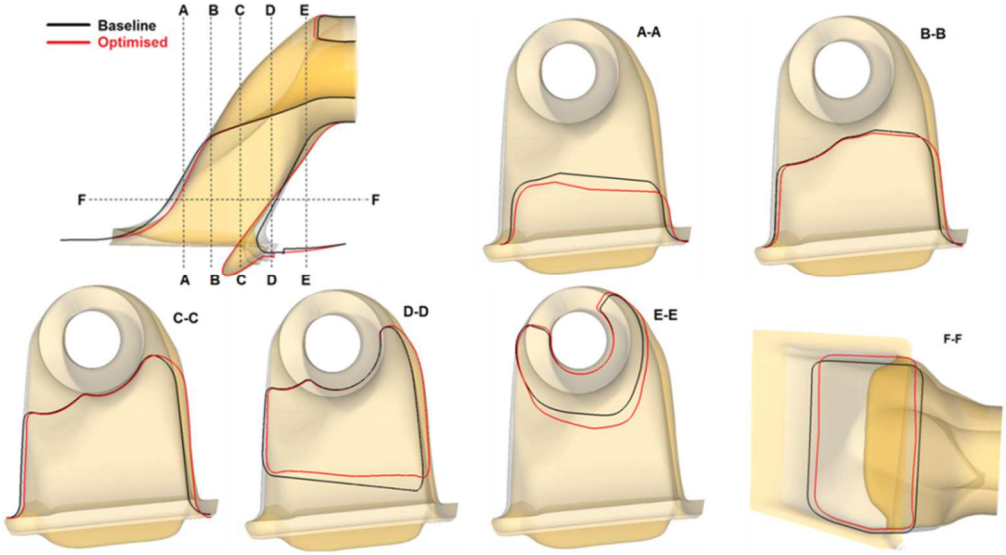


**Figure 17: Optimised shape of intake#2 compared to the baseline.**

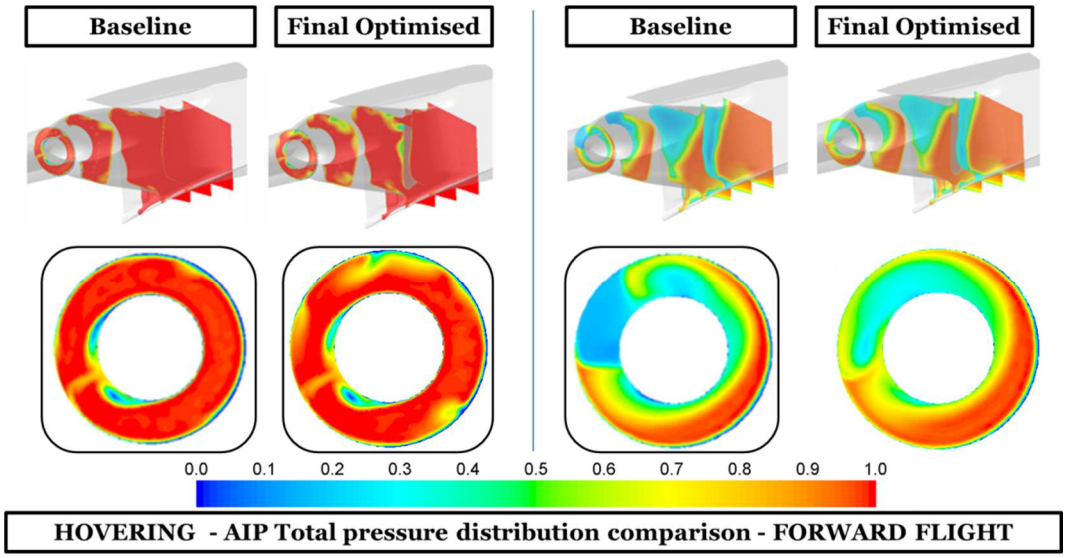


**Figure 18: Optimisation results on intake#2: total pressure losses along the optimised intake duct and over the AIP vs. baseline in hover (on the left) and cruise condition (on the right).**

between the baseline design and the selected optimised configuration of intake#2. The latter is characterized by a cross section shifted to the top direction (+z direction in the figures), which promotes a more efficient ingestion of the incoming air flow, at both flying conditions considered for optimization. The cross section surface extension appears to be nearly unchanged, also due to the strong front wall architectural constraint. As for intake#1, the front and rear wall curvatures are smoother than the baseline, thus reducing the severity of the S-bend and the turning angle of the incoming flow at cruise conditions. The presence of a protruding rear wall lip is helpful at cruise for the same reasons as for intake#1, and it results in a more uniform flow, but on the other hand it introduces an additional obstruction in the flow path at hover, which entails flow separation, especially on the top wall (Figure 18).

In general, the common geometrical features of the two optimized intakes are relevant, especially considering their different position over the fuselage, which implies two different incoming fluxes from the aerodynamic point of view. In fact, both the optimized intakes are characterized by a prominent rear lip fairing with a grown lip. This allows the air flow to be better conveyed thanks to the increase in static pressure levels in the stagnation region nearby the rear lip. Other common geometrical features of the two intakes are less pronounced front and rear wall curvatures which decrease the severity of S-shaped duct in terms of flow turning angles, leading to reduced extent and intensity of the separated flow region at the duct S-bend and a more uniform total pressure distribution at AIP.

**Exhaust Optimization.** After assessment of the baseline AW101 installation, the exhaust geometry was parameterized and the optimization problem formulation defined. Only the primary nozzle and the central body installed on Engine#2 were optimised. The shapes used for exhaust#2 optimization are shown in Figure 19. Unlike the intakes optimization, which was performed using a multi-point approach, the exhaust was optimized in a single flight condition using a multi-objective approach in the most relevant helicopter flight condition, i.e. cruise condition. The main objective was the minimization of engine back pressure, while the second objective was used to constraint the entrainment ratio to values close to the baseline, in order to meet the fire extinguishing system requirements. Specifically, the selected exhaust objective function E(x) was a bi-objective two component vector function, evaluated at the cruise condition only:

$$\text{minimize}\left\{E(x)=\begin{bmatrix} BP(x)\,|\,@\,cruise \\ \left|ER(x)-ER_{baseline}\right|\,|\,@\,cruise \end{bmatrix}\right\} \tag{6}$$

where *BP(x)* and *ER(x)* represent the back-pressure and the entrainment ratio respectively:

$$BP(x)=\frac{P_{T,exhaust-inlet}-P_s}{P_s};\; ER(x)=\frac{\dot{m}_{cold}(x)}{\dot{m}_{hot}} \tag{7}$$

where $P_s$ represents the free-stream static pressure.

Also in this case, a Design Of Experiments study was carried out for the exhaust in order to help in the selection of the final set of the parameters to be used in the optimization. The automatic optimization was then run until 5 genetic algorithm generations were completed, with 12 individuals per generation. Figure 20 shows the final Pareto frontier calculated by the GeDEA algorithm. The best configuration was finally selected among the solutions on the Pareto front: since obtained variations of entrainment ratio with respect to the baseline were considered to be acceptable, it was decided to privilege the maximum reduction in back pressure. Specifically, the selected optimal design is characterized by cruise total pressure loss reduction of 22.25% with respect to the baseline, while the difference between entrainment ratio of

optimized solution and the baseline is less than 4%, which was judged acceptable. The optimized geometry (see Figure 21) features a slightly longer nozzle than the baseline, the maximum allowed increase of equivalent exit area and a significant change in depth of flutes, combined with an extension of central body length. In particular, the deeper flutes and the larger exit diameter allow the exhaust flow to reduce the total back pressure and feature a better behavior in the mixing region which in turn causes a drop of exhaust average total temperature and core total temperature. In addition, it was verified that benefits in terms of back pressure reduction of the optimized configuration were transferred to ground-idle and hover as well, even though optimization was carried out in cruise conditions only: actually, a 30% reduction and a 10% reduction was achieved in ground-idle and in hover respectively with respect to the baseline. Regarding the entrainment ratio, the variation with respect to the baseline is slightly larger in ground idle than in cruise (5.7%), while in hover it is almost the same as in cruise (3.9%). The variations of entrainment ratio with respect to the baseline were in any case considered to be acceptable in agreement with AgustaWestland Ltd, so it was decided to retain the optimized solution with which the reduction of back pressure was privileged.

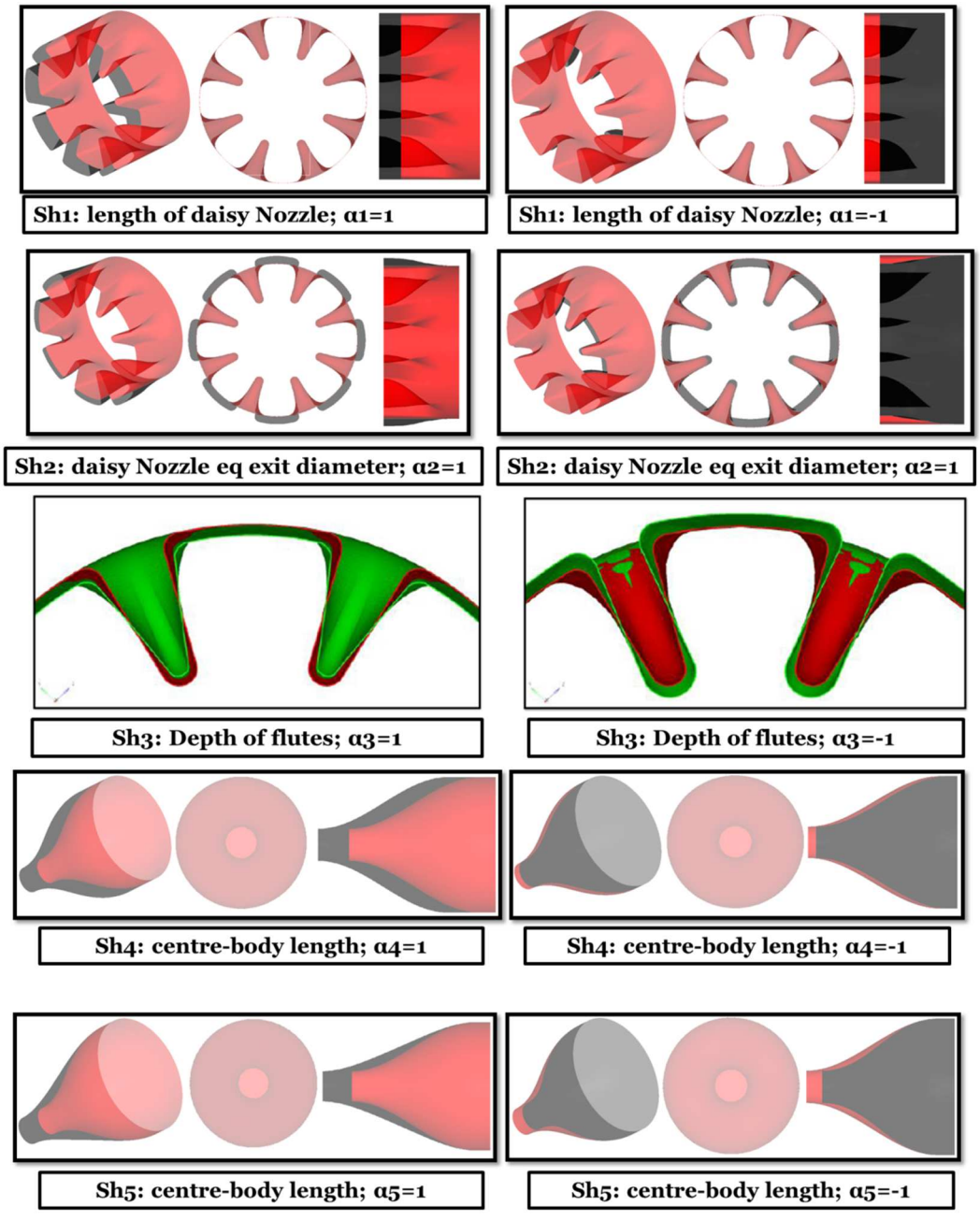


**Figure 19: Shapes used for optimization of exhaust#2.**

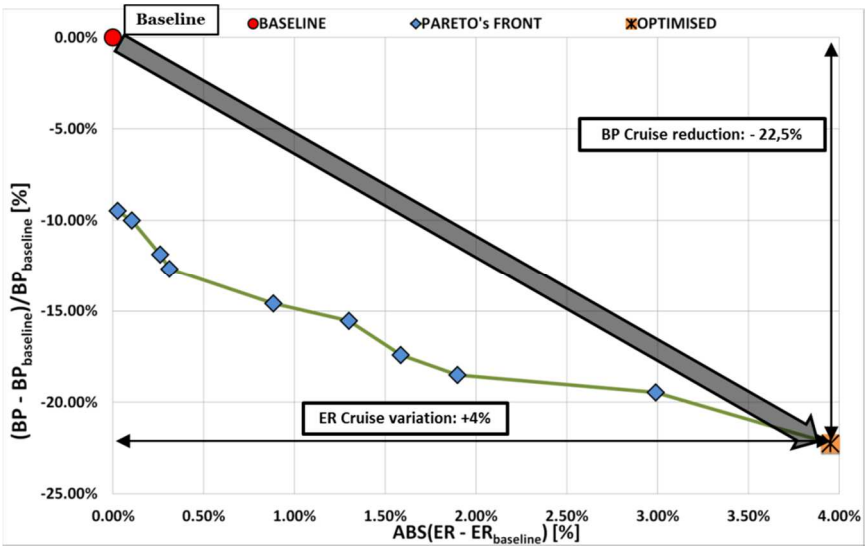


**Figure 20: Evolution of the Pareto front for optimization of exhaust#2.**

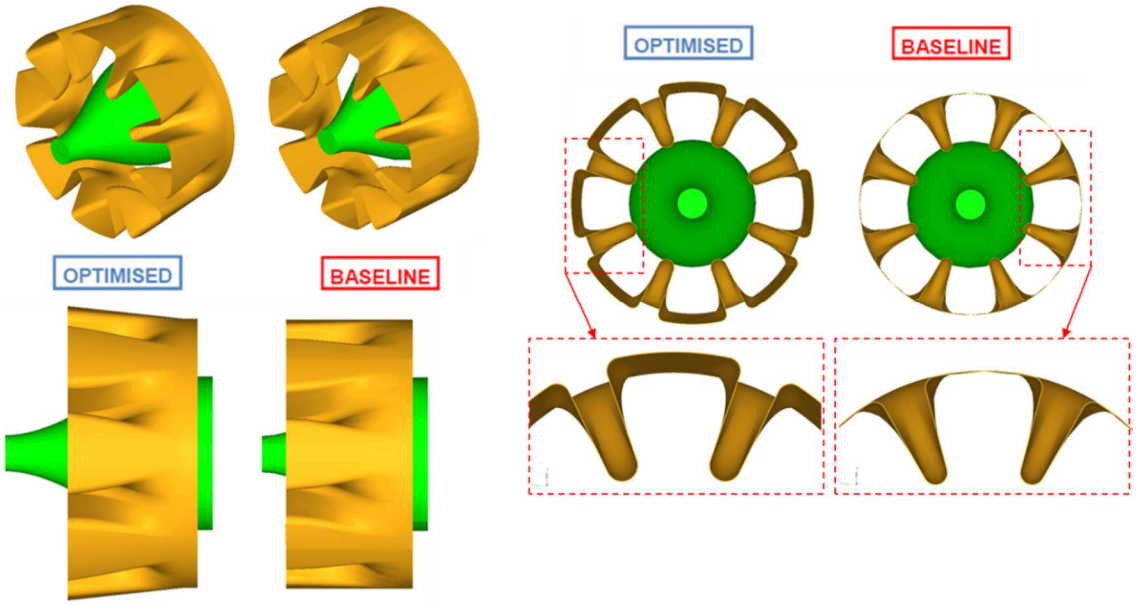


**Figure 21: Optimised shape of exhaust#2 compared to the baseline.**

Moreover, a meaningful reduction in the exhaust total temperature, especially in cruise, was found with the optimized solution, and also the turbulent viscosity was noticeably reduced in all the considered flight conditions. Also, the optimized geometry makes it possible to achieve an enhanced mixing of the hot and cold flows. This in turn is expected to be beneficial for the tail boom heating issue, since a more efficient mixing reduces the average temperature of the flow potentially impinging on the boom.

**Final Engine Installation Configuration.** The optimization of engine air intakes and exhaust identified the final optimized engine installation configurations for both AW101 engine#1 and engine#2. Then, a comprehensive characterization of the optimized solutions was carried out, aimed at assessing the aerodynamic behaviour of the whole helicopter with the new engine installation subsystems included into a single CFD model (Figure 22, Figure 23). In fact, the optimizations of intakes and exhaust were run using one numerical model per item. In particular, the helicopter aerodynamic performance was investigated in a number of operating regimes, such as forward flight, hovering, sideways and rearwards flight; moreover, an assessment of the rotor inflow effect in the intakes performance was carried out. Finally, some peculiar

issues of the engine installation were analyzed such as reverse flow into engine bay at ground-idle condition and potential drag and weight increase evaluation.

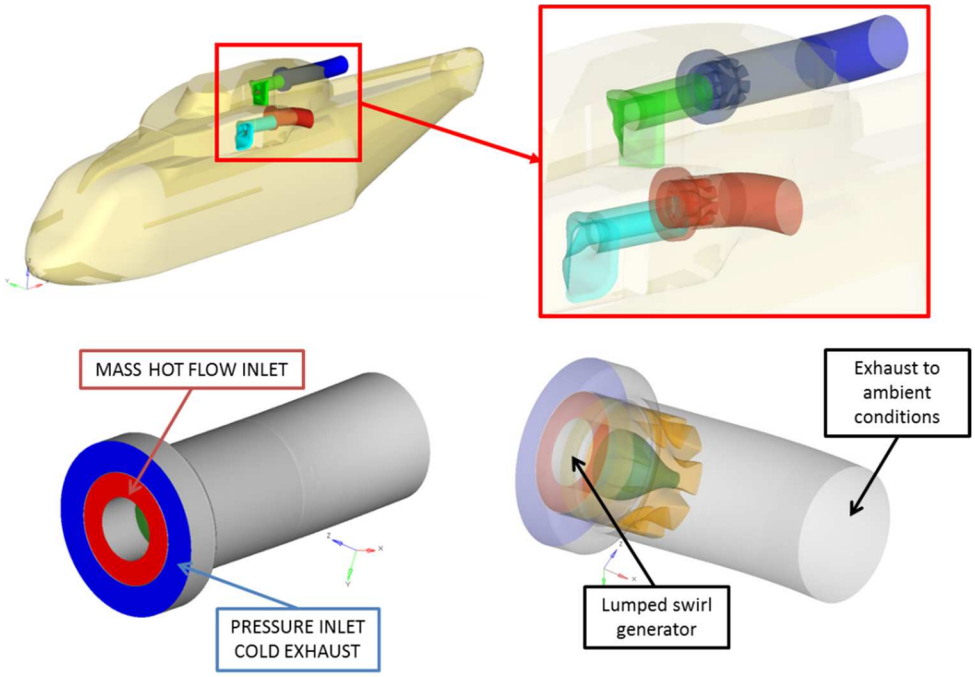


**Figure 22: Comprehensive model of the AW101 optimised engine installation.**

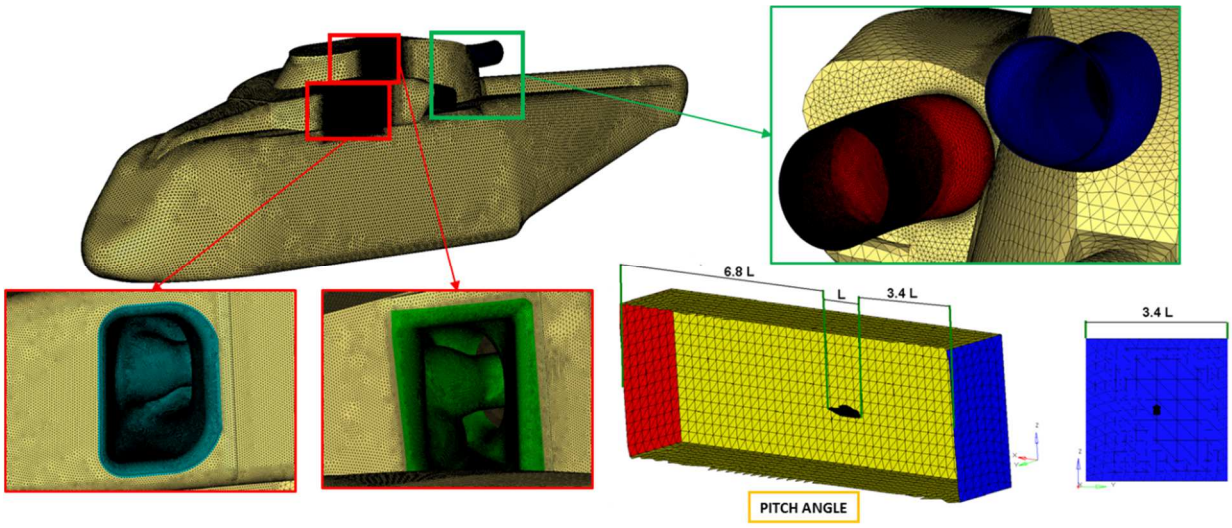


**Figure 23: Computational mesh of the comprehensive model of the AW101 optimised engine installation.**

First of all, the optimized exhaust performance on engine#1 was assessed: in fact, exhaust shape optimization was carried out in WP2 only on engine#2. However, since the exhaust#1 is the same as exhaust#2, apart from the geometry of secondary nozzle, it was expected that the optimization results on exhaust#2 could be directly transferred to exhaust#1. The basic features of the flow field of the optimized exhaust#1 system were compared against the baseline in terms of total pressure, total temperature and turbulent viscosity for three flight conditions of interest (i.e. forward flight, ground-idle and hover). The turbulent viscosity was noticeably reduced in all the considered conditions and a meaningful reduction in the exhaust total temperature, especially in cruise, was found. Similarly to the exhaust#2, the optimized geometry makes it possible to achieve an enhanced mixing of the hot and cold flows in exhaust#1. This in

turn is expected to be beneficial for the tail boom heating issue, since a more efficient mixing reduces the average temperature of the flow potentially impinging the boom. In addition, the global performance of the optimized exhaust in terms of both back pressure and entrainment ratio in the three considered flight conditions was analyzed and compared against the baseline. It was found that benefits in terms of back pressure reduction of the optimized configuration are transferred to exhaust#1 as well, even though to a lesser extent than exhaust#2. Actually, a 17% reduction, a 6% reduction and a 13% reduction was achieved in cruise, in ground-idle and in hover respectively with respect to the baseline. Regarding the entrainment ratio, the variation found with respect to the baseline was much larger than for exhaust#2, especially in cruise (23.3%), while it was still judged acceptable both in ground-idle (8.0%) and hover (2.0%). However, as for exhaust#2, also in this case the reduction of back pressure was privileged.

Then, the assessment of reverse flow into engine bay at ground idle conditions was carried out for both engine#1 and engine#2. As expected, the rearward wind condition causes the exhaust gases to be re-ingested into the pertinent engine bay (Figure 24). The comparison of baseline and optimized solutions for both exhaust#1 and exhaust#2 demonstrated that there are no significant differences between the baseline and the optimized geometries in both the engines. Obviously, the exhaust#1, whose secondary nozzle is shorter than exhaust#2, is more susceptible to external boundary conditions and, as a consequence, the exhausts re-ingestion is more pronounced. However, it was concluded that no detrimental effects with respect to the baseline were introduced by the optimization regarding this issue.

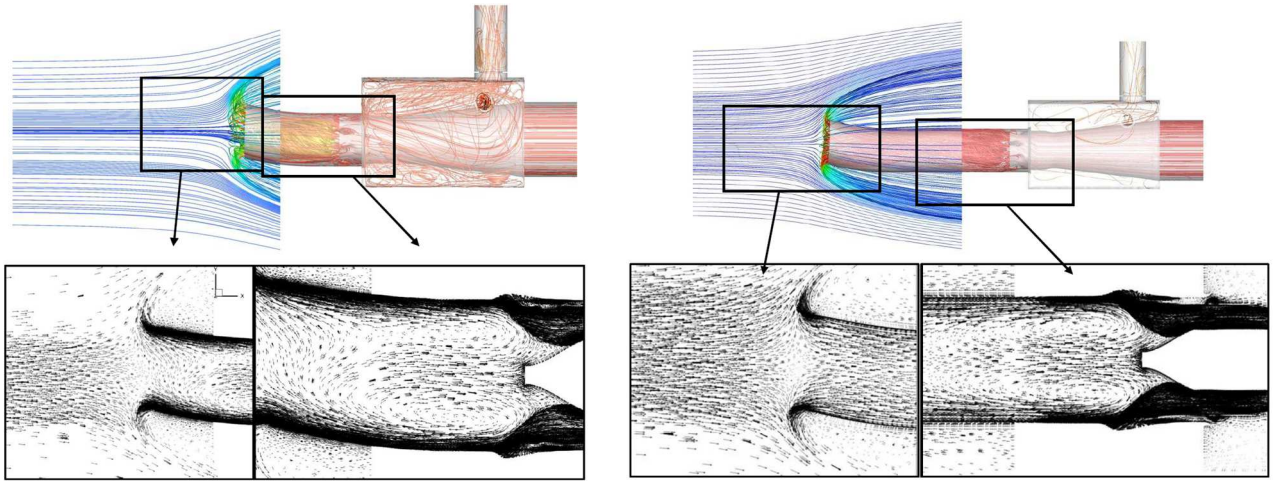

**Figure 24: Stream lines within the engine#1 (on the left) and engine#2 (on the right) bay and core exhaust pipe . Lines coloured by Total Temperature. Focus on the remix zone downstream of primary nozzle.**

Afterwards, the existing AW101 primary nozzle performance for exhaust#1 and exhaust#2 was analyzed in both cruise and ground-idle conditions. The current AW101 primary nozzle exhausts featured a totally different fluid-dynamic behavior in both cruise and ground idle flight conditions with respect to both the baseline and the optimized geometries. Specifically, a large perturbed region was observed in the central part of the core flow as a consequence of the abrupt step downstream of the primary nozzle which promotes flow separation. Furthermore, weaker mixing between the two flow streams is promoted by the de-swirl nozzle, whose geometry generates narrow mixing regions nearby the blades. Consequently, the comparison of current AW101 and the baseline rig exhaust showed that larger total temperature and smaller total pressure values are produced by the former in both the considered flight conditions, above all in ground idle, but with a different swirl for the exhaust flows that produces a noticeable reduction of the turbulent viscosity in all the considered flight conditions. On the other hand, the performance

improvement of the optimized geometries with respect to the current AW101 daisy nozzle was clearly appreciable: specifically, the reduction of back pressure in the optimized exhaust was clearly apparent in each of the considered flight conditions. In particular, an optimized backpressure equal to 2.06% was found for engine#1 in cruise conditions against 2.75% of the existing primary nozzle, while in ground idle the backpressure was the same for optimized and current solutions. For engine#2, a backpressure of 2.25% was found for the optimized solution against the 2.44% value of the current solution in cruise conditions, while in ground-idle the optimized exhaust featured a 0.25% backpressure against a 0.35% value for the current geometry. In addition, a meaningful reduction in the exhaust total temperature, especially in ground idle, was found, and also the turbulent viscosity was noticeably reduced in all the considered conditions.

Moreover, the effect of rotor inflow on the engine installation in cruise, hover, sideward and rearward flight was assessed for baseline and optimized daisy nozzle configurations. As far as cruise flight condition is concerned, the presence of the rotor inflow has a meaningful impact on the AIP total pressure distributions for both intake#1 and intake#2, both for baseline and optimized geometries. This is especially true for intake#2, whose total pressure contours are significantly modified in both baseline and optimized geometries as a consequence of the inclusion of the rotor effect. Specifically, the optimized intake#1 configuration exhibits a -30% drop in total pressure loss for rotor effects enabled and a -36% for rotor effects neglected, respectively. For intake#2, the selected geometry is characterized by a -14% reduction of total pressure loss in for rotor effects enabled, accompanied with a reduction of -26% for rotor effects neglected. Some differences were shown in both the intakes and for both the baseline and the optimized geometries with and without inclusion of the rotor effect for hovering condition as well, even if to a lower extent than for forward flight. Specifically, the optimized intake#1 configuration exhibits a -26% drop in total pressure loss for rotor effects enabled and a -24% for rotor effects neglected, respectively. For intake#2, the selected geometry is characterized by a -8% reduction of total pressure loss in for rotor effects enabled, accompanied with an increase of 5% for rotor effects neglected. For sideward cases, rotor effects were negligible. Specifically, the optimized intake#1 configuration exhibits a -14% drop in total pressure loss for rotor effects enabled and a -15% for rotor effects neglected, respectively. For intake#2, instead, the selected geometry is characterized by a 20% increment of total pressure loss in for rotor effects enabled, accompanied with an increase of 5% for rotor effects neglected. On the other hand, in rearward flight condition, significant differences were evidenced for the optimized intake#2. Specifically, the optimized intake#1 configuration exhibits a 2% increment in total pressure loss for rotor effects enabled and a 19% increment for rotor effects neglected, respectively. For intake#2, instead, the selected geometry is characterized by a 42% increment of total pressure loss in for rotor effects enabled, accompanied with an increase of 64% for rotor effects neglected.

As far as exhausts aerodynamic behavior is concerned, for cruise flight condition it was found that benefits in term of back pressure reduction of the optimized configuration are present for rotor effects enabled as well, even though with absolute values slightly higher in term of total pressure. Actually, a 19% reduction and a 11% reduction was achieved for exhaust#1 and exhaust#2 respectively for rotor effects neglected; a 13% reduction and a 12% reduction was achieved for exhaust#1 and exhaust#2 respectively for rotor effects enabled. Regarding the entrainment ratio, the variation found with respect to the baseline was much larger for exhaust#1 than for exhaust#2, especially for rotor effects neglected. The streamlines downstream of the exhausts are slightly deflected downwards when the rotor effect is considered and they seem to be more disturbed, while they are quite regular if the rotor inflow is not taken into account. For the hovering flight, benefits in term of back pressure reduction of the optimized configuration for both cases with rotor flow enabled and neglected are present as well. Actually, a 18% reduction and a 5% reduction was achieved for exhaust#1 and exhaust#2 respectively for rotor effects neglected; a 16% reduction and a 9% reduction was achieved for exhaust#1 and exhaust#2 respectively for rotor effects

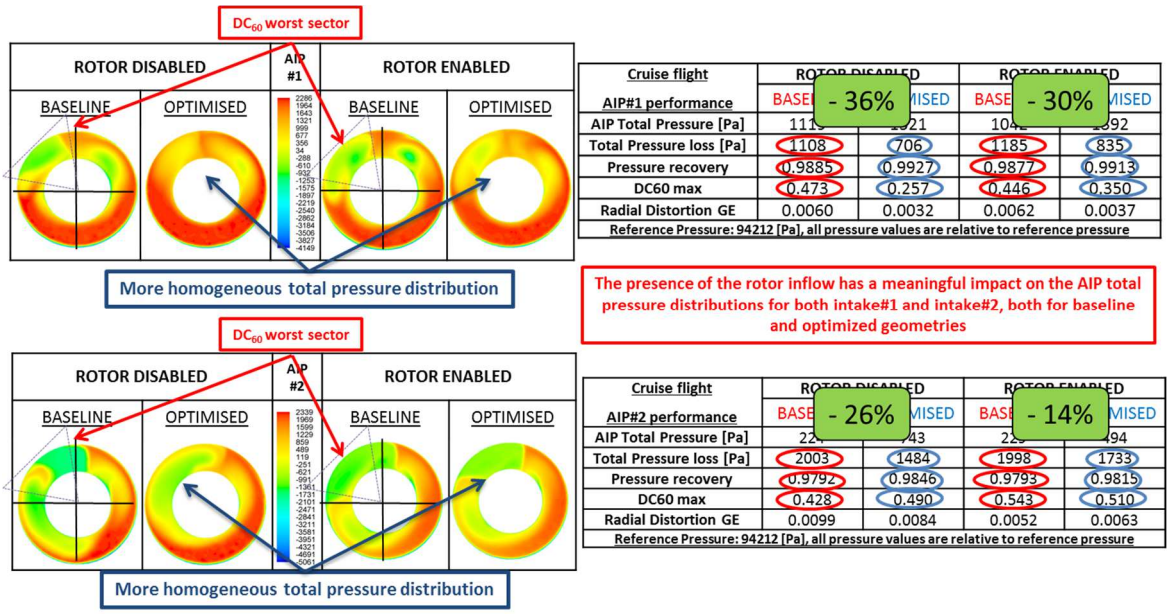


| Cruise flight | ROTOR DISABLED | | ROTOR ENABLED | |
|---|---|---|---|---|
| AIP#1 performance | BASE | - 36% MISED | BASE | - 30% MISED |
| AIP Total Pressure [Pa] | 111 | 21 | 104 | 92 |
| Total Pressure loss [Pa] | 1108 | 706 | 1185 | 835 |
| Pressure recovery | 0.9885 | 0.9927 | 0.9877 | 0.9913 |
| DC60 max | 0.473 | 0.257 | 0.446 | 0.350 |
| Radial Distortion GE | 0.0060 | 0.0032 | 0.0062 | 0.0037 |
| Reference Pressure: 94212 [Pa], all pressure values are relative to reference pressure | | | | |

The presence of the rotor inflow has a meaningful impact on the AIP total pressure distributions for both intake#1 and intake#2, both for baseline and optimized geometries

| Cruise flight | ROTOR DISABLED | | ROTOR ENABLED | |
|---|---|---|---|---|
| AIP#2 performance | BASE | - 26% MISED | BASE | - 14% MISED |
| AIP Total Pressure [Pa] | 22 | 43 | 22 | 94 |
| Total Pressure loss [Pa] | 2003 | 1484 | 1998 | 1733 |
| Pressure recovery | 0.9792 | 0.9846 | 0.9793 | 0.9815 |
| DC60 max | 0.428 | 0.490 | 0.543 | 0.510 |
| Radial Distortion GE | 0.0099 | 0.0084 | 0.0052 | 0.0063 |
| Reference Pressure: 94212 [Pa], all pressure values are relative to reference pressure | | | | |

**Figure 25: Effect of rotor inflow in forward flight: AIP total pressure contours [Pa] on baseline and optimised intake#1 (top) and intake#2 (bottom).**

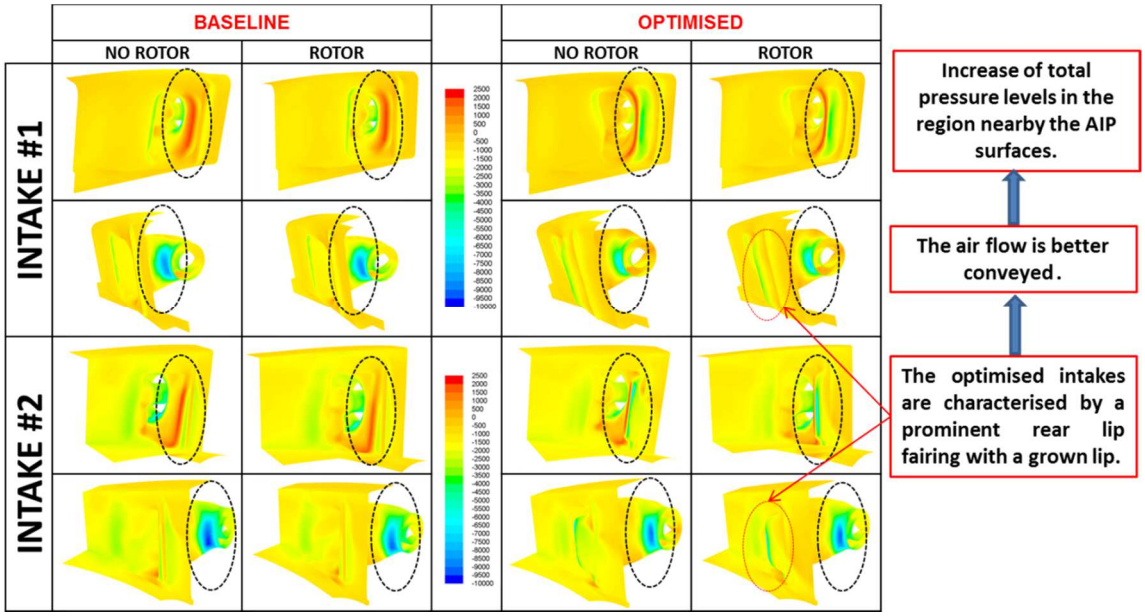


**Figure 26: Effect of rotor inflow in forward flight: Total pressure contours [Pa] on baseline and optimised intake#1 (top) and intake#2 (bottom).**

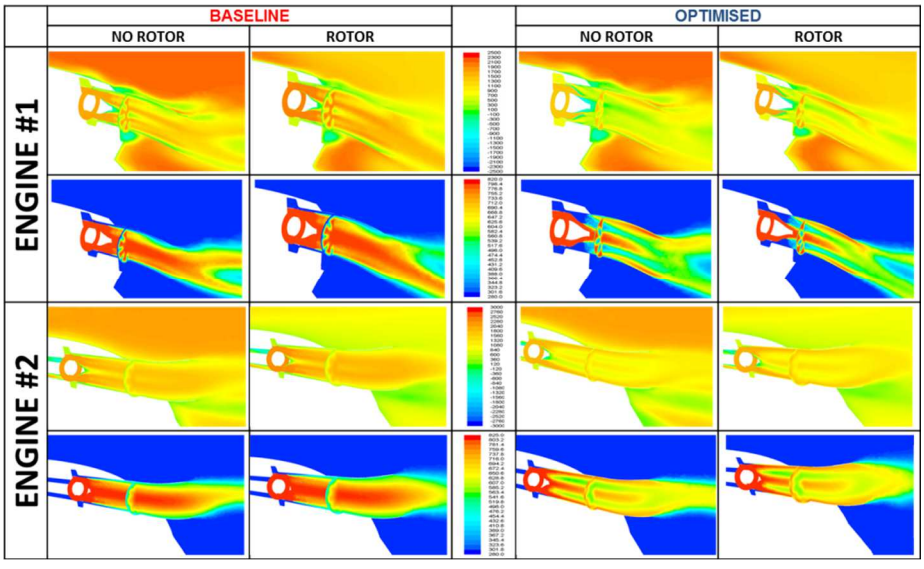


**Figure 27: Effect of rotor inflow in forward flight: Total pressure contours [Pa] (top) and total temperature contours [K] (bottom) on baseline and optimised exhaust#1 and exhaust#2.**

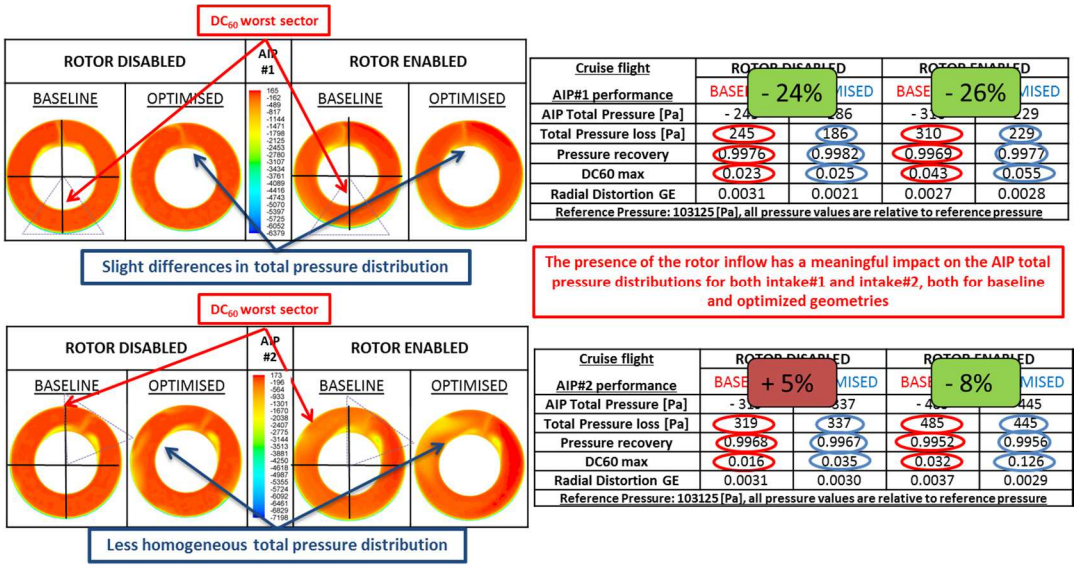


| Cruise flight | ROTOR DISABLED | | ROTOR ENABLED | |
|---|---|---|---|---|
| AIP#1 performance | BASE | - 24% MISED | BASE | - 26% MISED |
| AIP Total Pressure [Pa] | - 24 | 86 | - 31 | 29 |
| Total Pressure loss [Pa] | 245 | 186 | 310 | 229 |
| Pressure recovery | 0.9976 | 0.9982 | 0.9969 | 0.9977 |
| DC60 max | 0.023 | 0.025 | 0.043 | 0.055 |
| Radial Distortion GE | 0.0031 | 0.0021 | 0.0027 | 0.0028 |
| Reference Pressure: 103125 [Pa], all pressure values are relative to reference pressure | | | | |

The presence of the rotor inflow has a meaningful impact on the AIP total pressure distributions for both intake#1 and intake#2, both for baseline and optimized geometries

| Cruise flight | ROTOR DISABLED | | ROTOR ENABLED | |
|---|---|---|---|---|
| AIP#2 performance | BASE | + 5% MISED | BASE | - 8% MISED |
| AIP Total Pressure [Pa] | - 31 | 37 | - 4 | 445 |
| Total Pressure loss [Pa] | 319 | 337 | 485 | 445 |
| Pressure recovery | 0.9968 | 0.9967 | 0.9952 | 0.9956 |
| DC60 max | 0.016 | 0.035 | 0.032 | 0.126 |
| Radial Distortion GE | 0.0031 | 0.0030 | 0.0037 | 0.0029 |
| Reference Pressure: 103125 [Pa], all pressure values are relative to reference pressure | | | | |

**Figure 28: Effect of rotor inflow in hover: AIP total pressure contours [Pa] on baseline and optimised intake#1 (top) and intake#2 (bottom).**

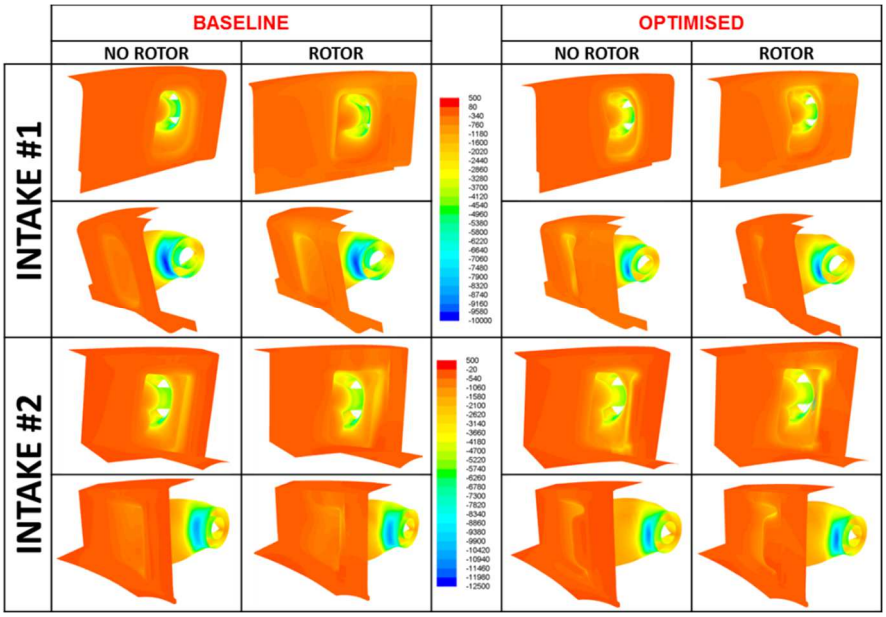


**Figure 29: Effect of rotor inflow in hover: Total pressure contours [Pa] on baseline and optimised intake#1 (top) and intake#2 (bottom).**

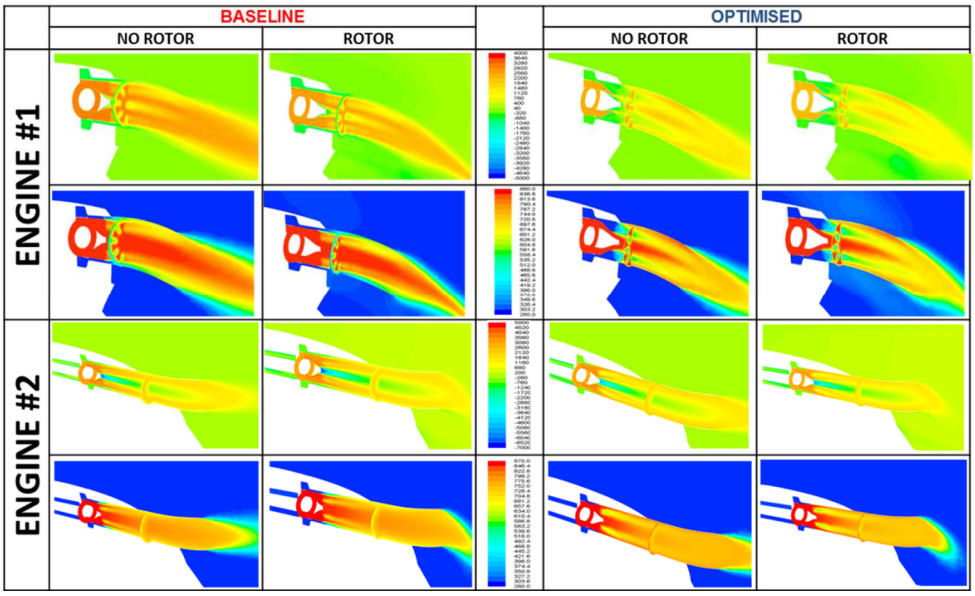


**Figure 30: Effect of rotor inflow in hover: Total pressure contours [Pa] (top) and total temperature contours [K] (bottom) on baseline and optimised exhaust#1 and exhaust#2.**

enabled. Regarding the entrainment ratio, the variation found with respect to the baseline was much larger for exhaust#1 than for exhust#2 as well. On the other hand, much more apparent are the differences in the exhausts fluid-dynamic behavior for the presence of the rotor. As expected, the rotor inflow in hover is the main driver for the exhaust plume trajectory in both the baseline and the optimized geometries: actually, streamlines downstream of the exhausts are diverted downstream by the rotor inflow. The benefits in term of back pressure reduction of the optimized configuration for both cases with rotor flow enabled and neglected are present for sideward and rearward flight conditions as well. For sideward flight, a 17% reduction and a 8% reduction was achieved for exhaust#1 and exhaust#2 respectively for rotor effects neglected; a 16% reduction and a 4% reduction was achieved for exhaust#1 and exhaust#2 respectively for rotor effects enabled. Also in this case, including the rotor inflow directly influences the exhausts streamlines path: actually, streamlines are deflected downwards when the rotor is enabled for both the baseline and the optimized geometries, while they are deflected upwards when the rotor is neglected, especially for the baseline geometry. When the optimized exhausts are considered without the presence of the rotor, the exhausts of engine#1 impinge on the fuselage tail, so this issue has to be taken into account when considering tail boom heating. For rearward flight, a 18% reduction and a 6% reduction was achieved for exhaust#1 and exhaust#2 respectively for rotor effects neglected; a 15% reduction and a 4% reduction was achieved for exhaust#1 and exhaust#2 respectively for rotor effects enabled. The rearward wind condition causes the exhaust gases to be re-ingested into the pertinent engine bay. Also, the comparison of baseline and optimized solutions for both exhaust#1 and exhaust#2 demonstrates that there are significant differences in the intakes performance if the rotor effect is included; in particular, the re-ingestion of the exhaust gases does not occur when the rotor is enabled because of the additional velocity component in the vertical direction induced by the rotor, that helps moving away from the fuselage the exhaust gases. Based on the achieved results, it was concluded that no meaningful differences in the performance parameters for intakes and exhausts used for optimization are introduced when the rotor inflow effects are considered. Effects of rotor inflow in forward flight and hover are illustrated in Figures 25-30, where the AIP total pressure contours, total pressure contours over the intakes and total pressure and temperature field downstream the exhaust are depicted for both baseline and optimised configurations, both with rotor inflow included and neglected from the simulations.

A comprehensive quantification of overall margins of improvement of the optimised engine installation with respect to the baseline for the representative flight conditions analysed is given in Figures 31-45, where the total pressure losses, pressure recovery, DC60 maximum value, GE distortion parameter, exhaust inlet total pressure, backpressure and entrainment ratio of the optimised installation are illustrated and compared against the baseline, both with and without rotor included. The same results are summarized in quantitative form in Table 1.

A weight assessment was carried out for the optimised engine installation, and it was found that the optimised intake#1 and intake#2 areas were increased by 20% and 8.5% respectively with respect to baseline, while the primary nozzle and central body were increased by 9.5% and 25.6% respectively with respect to the baseline. However, this corresponds to a very small overall weight increment of around 4 kg, which was considered acceptable.

As far as drag is concerned, as expected, the optimized engine installation featured a drag increment in cruise condition, mainly due to the rear lip introduced in the optimized intakes: the estimated increment was around 2% for the simplified, tail-off fuselage considered in the simulations, but percentage variation is expected to lower when the whole fuselage surfaces are to be included in the calculations. On the other hand, the optimization was found to induce a drag reduction both in sideward and rearward flight, both with the rotor effect included and neglected. However, it has to be kept in mind that this is only a quite rough estimation, since the hover rotor inflow was used for sideward and rearward flight conditions as well, rather than the pertinent inflow, for simplicity reasons.

In addition to DC60, another metrics for intake distortion quantification, namely the so-called "GE distortion parameter" was calculated for both intake#1and intake#2 in both forward flight and hover conditions. Regarding intake#1, both the GE circumferential and radial distortion parameters on the AIP surface showed that the geometry modifications carried out during the optimization induce a much more uniform total pressure distribution over AIP with a lower level of distortion in cruise condition. Actually, the optimized geometry features a maximum value of the GE radial distortion parameter equal to 0.199 against the baseline value of 0.509. This holds true also for hover, even though differences are smaller than in forward flight condition: in fact, the optimized geometry features a maximum value of the GE radial distortion parameter equal to 0.791 against the baseline value of 0.817. Regarding intake#2, the AIP total pressure contours featured a more uniform distribution with a lower level of distortion in cruise flight condition. Even though flow at intake#2 AIP is intrinsically much less uniform than for intake#1, optimization leads to meaningful improvements. Actually, the maximum value of the GE radial distortion parameter of optimized intake is equal to 1.078 against the value of 4.186 given for the baseline geometry. Finally, in hover flight condition, the optimized intake#2 geometry features a much less pronounced reduction of the GE circumferential distortion parameters than for cruise: however, the maximum value of the GE radial distortion parameter for optimized geometry AIP is lower than baseline geometry, being it equal to 0.772 against the baseline value of 0.827.

Finally, pressure loads were assessed both over the intakes and exhaust in both forward flight and hover for structural feasibility considerations. Regarding intake#1, maximum variations of about -5/+5% and of about -1.5/+3% were evidenced in cruise and hover flight conditions respectively with respect to the baseline. As expected, the most significant differences were shown on the rear-lip and on the rear S-duct surface, whose shapes changes were more pronounced in the optimization process. The same holds true for intake#2, where maximum variations of about -10/+5% and of about -3/+4% were found in cruise and hover flight conditions respectively with respect to the baseline. Finally, regarding the exhaust, variations of -2/+2% and of -8/+7% were shown in cruise and hover flight conditions respectively with respect to the baseline. In particular, benefits in terms of back pressure reduction of the optimized configuration are apparent; actually, the total pressure on internal surface of the optimized primary nozzle is lower than the baseline geometry in both flight conditions.

The major conclusions of the HEAVYcOPTer program are summarized in the following:

- The applicability and effectiveness of the GeDEA-driven optimization loop in addressing the aerodynamic optimization of the AW101 heavy class helicopter engine intakes and exhausts was widely demonstrated.

- The intakes under consideration are two out of the three that characterise the engine installation of the AW101 helicopter: intake#1, located at the left pilot's side, and intake#2, located on the top and next to the roof. The optimization carried out on intakes made it possible to achieve remarkable improvements on the main performance parameters and to obtain an enhanced intake aerodynamic behaviour. Specifically, the optimised intake#1 configuration exhibits a -25% drop in total pressure loss in hover and a -33% reduction in cruise, respectively. For intake#2, the selected geometry is characterised by a -25% reduction of total pressure loss in forward flight, accompanied with an increment of 11% at hovering. In addition, both the intakes are compliant with the flow distortion functional constraint at forward flight conditions.

- Optimization was carried out on the exhaust#2 (central engine) as well. Actually, since exhaust#1 is the same as exhaust#2, apart from the geometry of the secondary nozzle, it was believed that optimization results on exhaust#2 could be transferred directly to exhaust#1. The main objective

was the minimization of engine back pressure, while the second objective was used to constraint the entrainment ratio to values close to the baseline, in order to meet the fire extinguishing system requirements. The best configuration was selected among the solutions on the Pareto front: since variations of entrainment ratio with respect to the baseline were considered to be acceptable, it was decided to privilege the maximum reduction in back pressure. Specifically, the selected optimal design is characterized by cruise total pressure loss reduction of 22.25% with respect to the baseline, while the difference between entrainment ratio of optimized solution and the baseline is less than 4%.

- A comprehensive characterization of the optimised solutions for AW101 engine intakes and exhausts was then carried out in various flight conditions, with the purpose of estimating the overall aerodynamic behaviour of the whole engine installation using a single and all-inclusive CFD model. In particular, the aerodynamic performance of the optimised AW101 engine installation was examined in cruise, hovering, sideward and rearward flight and the effects of rotor inflow were assessed as well. Based on the achieved results, it was concluded that no meaningful differences in the performance parameters for intakes and exhausts used for optimization are introduced when the rotor inflow effects are considered.

- Regarding the weight assessment, the optimised intake#1 and intake#2 areas were increased by 20% and 8.5% respectively with respect to baseline, while the primary nozzle and central body were increased by 9.5% and 25.6% respectively with respect to the baseline. However, this corresponds to a very small overall weight increment of around 2 kg, which is considered acceptable.

- One main drawback is identified as far as drag is concerned. As expected, the optimized engine installation featured a drag increment in cruise condition, mainly due to the rear lip introduced in the optimized intakes: the estimated increment was around 2% for the simplified, tail-off fuselage considered in the simulations, but percentage variation is expected to lower when the whole fuselage surfaces are to be included in the calculations. On the other hand, the optimization was found to induce a drag reduction both in sideward and rearward flight, both with the rotor effect included and neglected. However, it has to be kept in mind that this is only a quite rough estimation, since the hover rotor inflow was used for sideward and rearward flight conditions as well, rather than the pertinent inflow, for simplicity reasons.

- Finally, pressure loads were assessed both over the intakes and exhaust in both forward flight and hover for structural feasibility considerations. Regarding both intakes, negligible variations were evidenced. As expected, the most significant differences were shown on the rear-lip and on the rear S-duct surface, whose shapes changes were more pronounced in the optimisation process. On the other hand, regarding the exhaust, benefits in terms of back pressure reduction of the optimized configuration are apparent; actually, the total pressure on internal surface of the optimised primary nozzle is lower than the baseline geometry in both flight conditions.

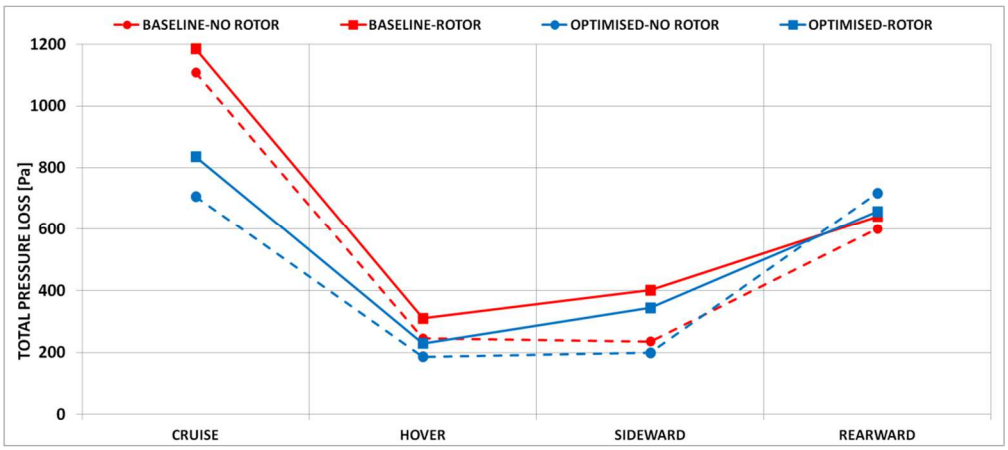


**Figure 31: AIP total pressure loss [Pa] values comparison for intake#1 designs.**

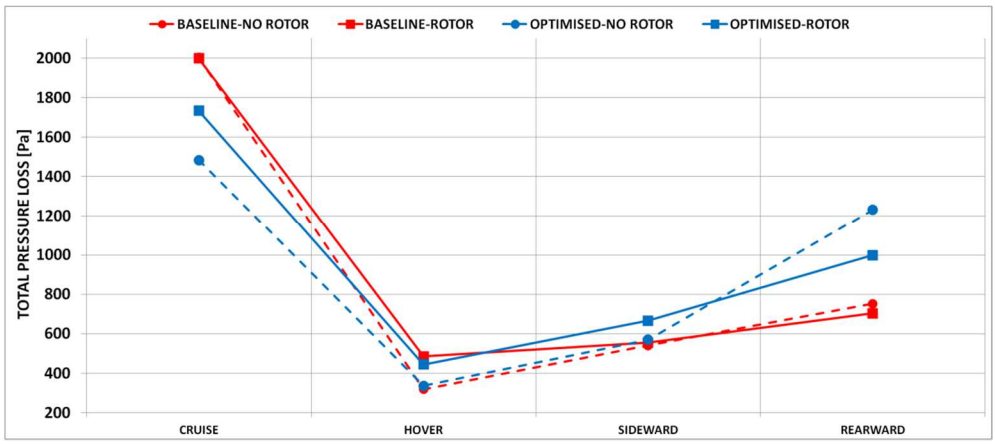


**Figure 32: AIP total pressure loss [Pa] values comparison for intake#2 designs.**

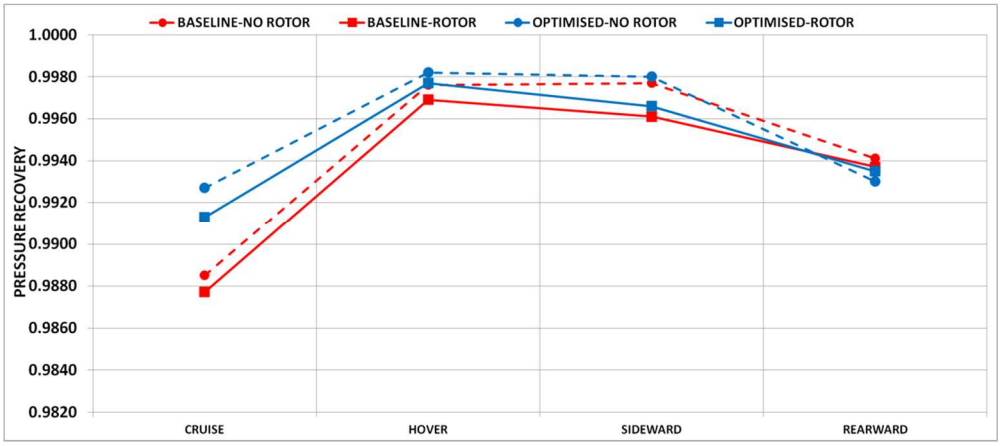


**Figure 33: AIP pressure recovery values comparison for intake#1 designs.**

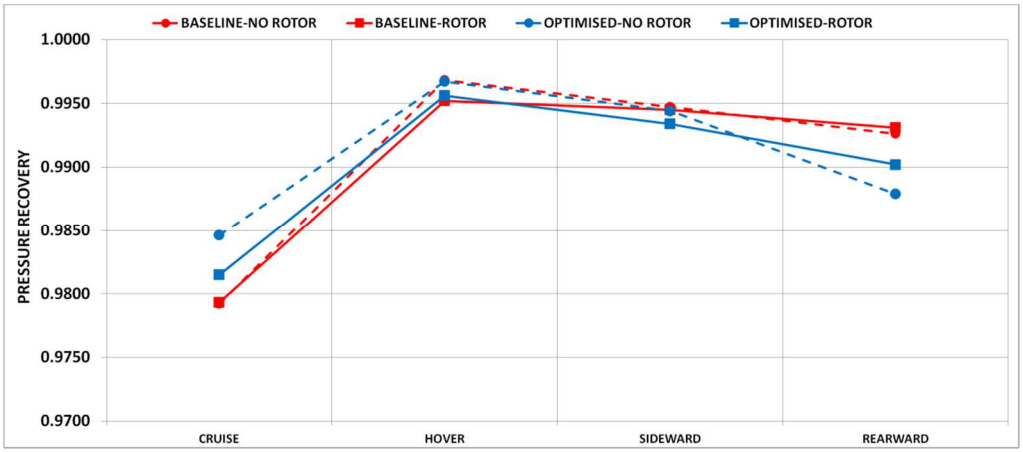


**Figure 34: AIP pressure recovery values comparison for intake#2 designs.**

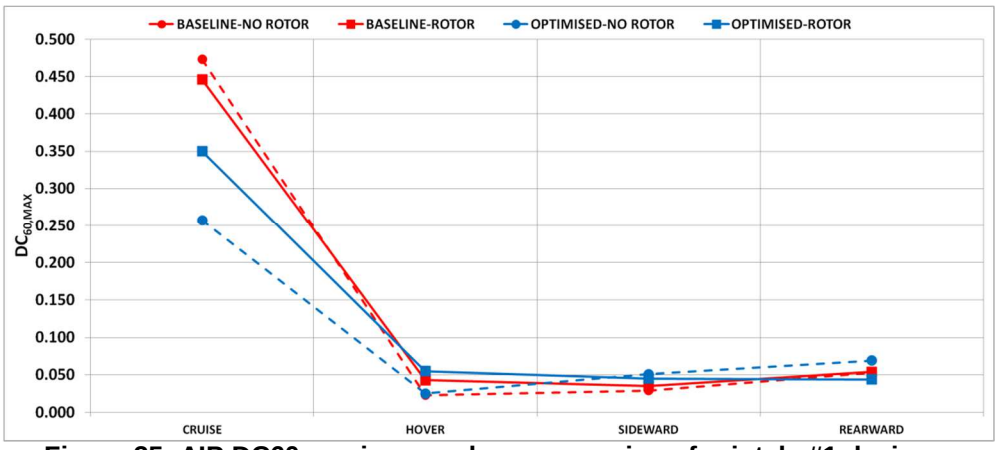


**Figure 35: AIP DC60 maximum values comparison for intake#1 designs.**

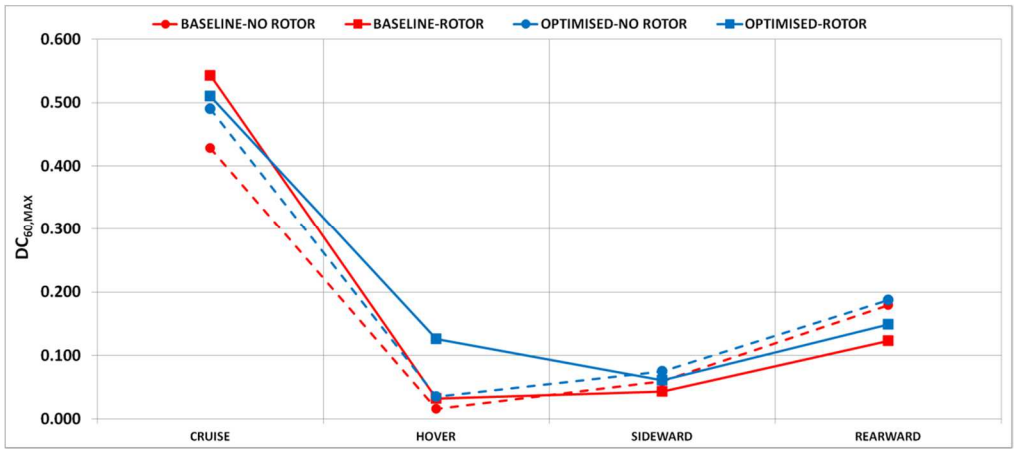


**Figure 36: AIP DC60 maximum values comparison for intake#2 designs.**

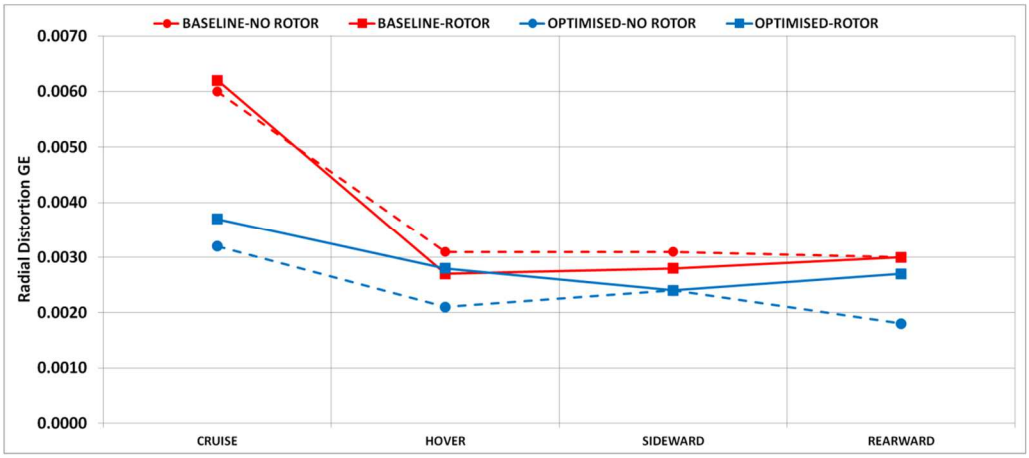


**Figure 37: AIP radial distortion GE parameter values comparison for intake#1 designs.**

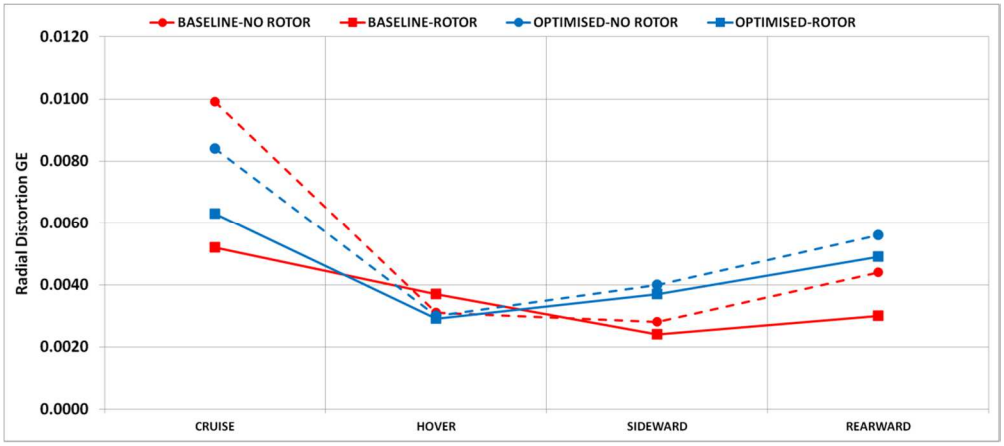


**Figure 38: AIP radial distortion GE parameter values comparison for intake#2 designs.**

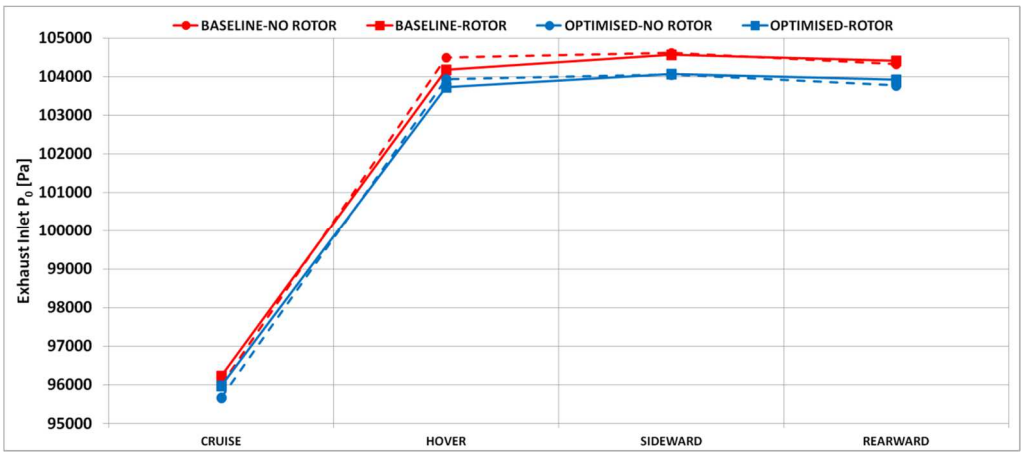


**Figure 39: Exhaust#1 inlet total pressure [Pa] values comparison.**

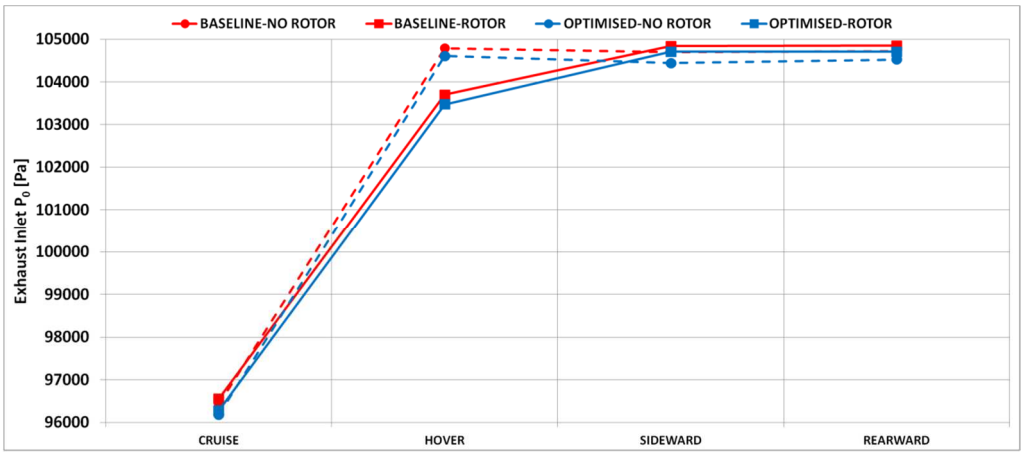


**Figure 40: Exhaust#2 inlet total pressure [Pa] values comparison.**

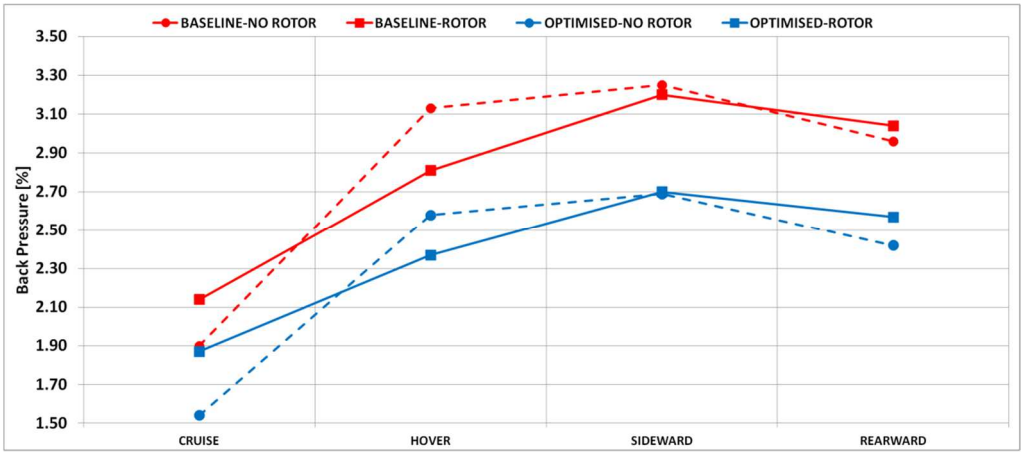


**Figure 41: Exhaust#1 Back Pressure values comparison.**

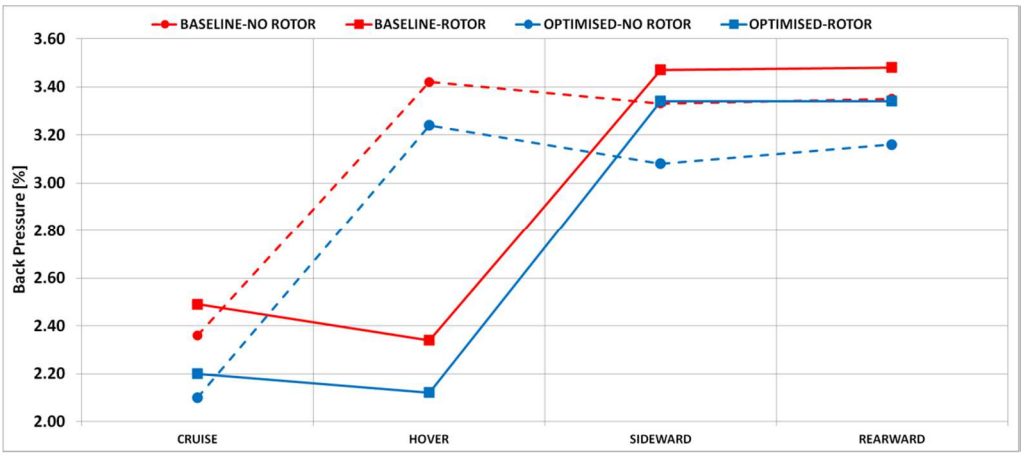


**Figure 42: Exhaust#2 Back Pressure values comparison.**

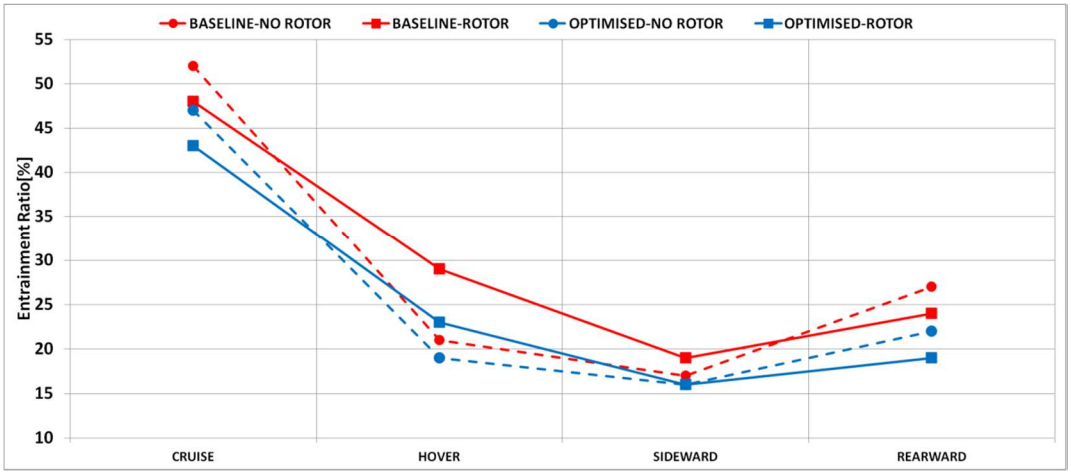


**Figure 43: Exhaust#1 Entrainment Ratio values comparison.**

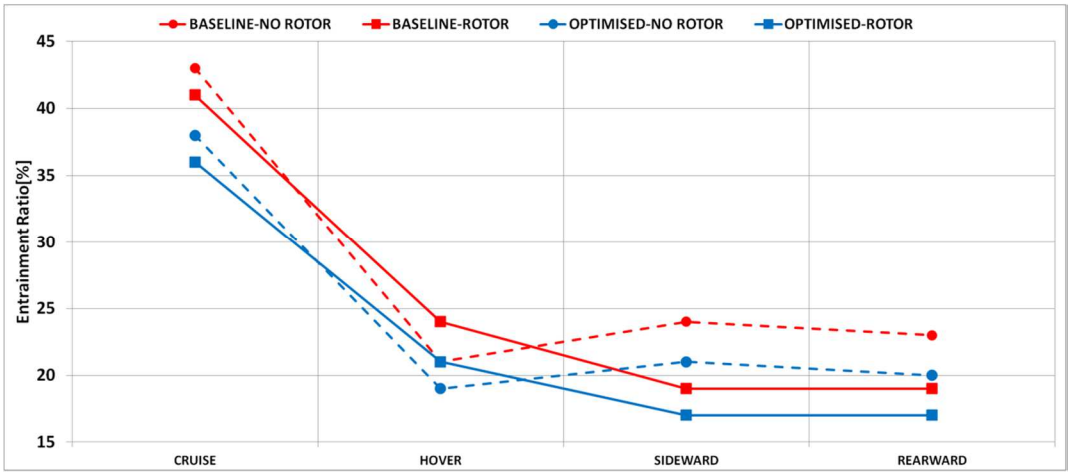


**Figure 44: Exhaust#2 Entrainment Ratio values comparison.**

| | ENGINE #1 | | | | | | | ENGINE #2 | | | | | | |
|---|---|---|---|---|---|---|---|---|---|---|---|---|---|---|
| | CRUISE | | | | | | | CRUISE | | | | | | |
| | TP loss[Pa] | PR | DC60 | GE | inletP0 [Pa] | BP [%] | ER [%] | TP loss[Pa] | PR | DC60 | GE | inletP0 [Pa] | BP [%] | ER [%] |
| BASELINE-NO ROTOR | 1108 | 0.9885 | 0.473 | 0.0060 | 96002 | 1.90 | 52 | 2003 | 0.9792 | 0.428 | 0.0099 | 96432 | 2.36 | 43 |
| BASELINE-ROTOR | 1185 | 0.9877 | 0.446 | 0.0062 | 96227 | 2.14 | 48 | 1998 | 0.9793 | 0.543 | 0.0052 | 96562 | 2.49 | 41 |
| OPTIMISED-NO ROTOR | 706 | 0.9927 | 0.257 | 0.0032 | 95667 | 1.54 | 47 | 1484 | 0.9846 | 0.490 | 0.0084 | 96187 | 2.10 | 38 |
| OPTIMISED-ROTOR | 835 | 0.9913 | 0.350 | 0.0037 | 95972 | 1.87 | 43 | 1733 | 0.9815 | 0.510 | 0.0063 | 96287 | 2.20 | 36 |
| | | | | | | | | | | | | | | |
| | HOVER | | | | | | | HOVER | | | | | | |
| | TP loss[Pa] | PR | DC60 | GE | inletP0 [Pa] | BP [%] | ER [%] | TP loss[Pa] | PR | DC60 | GE | inletP0 [Pa] | BP [%] | ER [%] |
| BASELINE-NO ROTOR | 245 | 0.9976 | 0.023 | 0.0031 | 104495 | 3.13 | 21 | 319 | 0.9968 | 0.016 | 0.0031 | 104790 | 3.42 | 21 |
| BASELINE-ROTOR | 310 | 0.9969 | 0.043 | 0.0027 | 104175 | 2.81 | 29 | 485 | 0.9952 | 0.032 | 0.0037 | 103700 | 2.34 | 24 |
| OPTIMISED-NO ROTOR | 186 | 0.9982 | 0.025 | 0.0021 | 103935 | 2.58 | 19 | 337 | 0.9967 | 0.035 | 0.0030 | 104610 | 3.24 | 19 |
| OPTIMISED-ROTOR | 229 | 0.9977 | 0.055 | 0.0028 | 103725 | 2.37 | 23 | 445 | 0.9956 | 0.126 | 0.0029 | 103475 | 2.12 | 21 |
| | | | | | | | | | | | | | | |
| | SIDEWARD | | | | | | | SIDEWARD | | | | | | |
| | TP loss[Pa] | PR | DC60 | GE | inletP0 [Pa] | BP [%] | ER [%] | TP loss[Pa] | PR | DC60 | GE | inletP0 [Pa] | BP [%] | ER [%] |
| BASELINE-NO ROTOR | 235 | 0.9977 | 0.029 | 0.0031 | 104615 | 3.25 | 17 | 541 | 0.9947 | 0.059 | 0.0028 | 104695 | 3.33 | 24 |
| BASELINE-ROTOR | 401 | 0.9961 | 0.035 | 0.0028 | 104570 | 3.20 | 19 | 555 | 0.9945 | 0.043 | 0.0024 | 104845 | 3.47 | 19 |
| OPTIMISED-NO ROTOR | 199 | 0.9980 | 0.051 | 0.0024 | 104055 | 2.69 | 16 | 570 | 0.9944 | 0.075 | 0.0040 | 104445 | 3.08 | 21 |
| OPTIMISED-ROTOR | 344 | 0.9966 | 0.045 | 0.0024 | 104065 | 2.70 | 16 | 667 | 0.9934 | 0.061 | 0.0037 | 104705 | 3.34 | 17 |
| | | | | | | | | | | | | | | |
| | REARWARD | | | | | | | REARWARD | | | | | | |
| | TP loss[Pa] | PR | DC60 | GE | inletP0 [Pa] | BP [%] | ER [%] | TP loss[Pa] | PR | DC60 | GE | inletP0 [Pa] | BP [%] | ER [%] |
| BASELINE-NO ROTOR | 600 | 0.9941 | 0.053 | 0.0030 | 104325 | 2.96 | 27 | 752 | 0.9926 | 0.179 | 0.0044 | 104723 | 3.35 | 23 |
| BASELINE-ROTOR | 641 | 0.9937 | 0.054 | 0.0030 | 104405 | 3.04 | 24 | 704 | 0.9931 | 0.123 | 0.0030 | 104855 | 3.48 | 19 |
| OPTIMISED-NO ROTOR | 717 | 0.9930 | 0.069 | 0.0018 | 103775 | 2.42 | 22 | 1232 | 0.9879 | 0.187 | 0.0056 | 104525 | 3.16 | 20 |
| OPTIMISED-ROTOR | 657 | 0.9935 | 0.044 | 0.0027 | 103925 | 2.57 | 19 | 998 | 0.9902 | 0.149 | 0.0049 | 104705 | 3.34 | 17 |

**Table 1: Summary of several performance indexes for baseline and optimised engines designs for both cases with rotor flow enabled and neglected.**

**References**


[1] Farokhi, S., (2008), *Aircraft Propulsion*, John Wiley & Sons.

[2] Cumpsty N.A., (1989), *Compressor Aerodynamics*, Longman.

[3] Vuillet A., (1980), *Aerodynamic Design of Engine Air Intakes for Improved Performance*, Sixth European Rotorcraft and Power Lift Aircraft Forum, Bristol.

[4] Breuer T., Bissinger N. C., (2010), *Basic Principles - Gas Turbine Compatibility - Intake Aerodynamic Aspects*, Encyclopedia of Aerospace Engineering, Vol. 8, Chapter EAE487

[5] Toffolo, A., Benini, E., *Genetic diversity as an objective in multi-objective evolutionary algorithms*. Evolutionary Computation, MIT press journal, 11(2):151–167, 2003.


| | | |
|---|---|---|
| Participating members | UNIVERSITY OF PADOVA | IT |
| | HIT09 S.r.l. | IT |
| | MDA S.r.l. | IT |


Coordinator contact details: Ernesto Benini

✉ Via Venezia, no.1

35131 Padova

Italy

☎ +39 (0)49 8276767

ernesto.benini@unipd.it

Technical Leader contact details: Rita Ponza

✉ Galleria Storione, no.8

35100 Padova

Italy

☎ +39 (0)333 2900558

r.ponza@hit09.com

**DESCRIPTION OF THE POTENTIAL IMPACT (INCLUDING THE SOCIO-ECONOMIC IMPACT AND THE WIDER SOCIETAL IMPLICATIONS OF THE PROJECT SO FAR) AND THE MAIN DISSEMINATION ACTIVITIES AND THE EXPLOITATION OF RESULTS**

The HEAVYcOPTer project is expected to result in a series of environmental benefits: in fact, a better engine installation will ultimately lead to an increase in the engine global efficiency and hence in reducing fuel consumption for the required levels of thrust. On the other hand, if a global reduction in the required thrust level is to be achieved as a result of the overall GRC project – by virtue of a possible aircraft drag reduction - the HEAVYcOPTer project will result in even more evident fuel savings. Actual quantification of benefits in terms of fuel saving has not yet been carried out being out of the scope of the project but it will be estimated within GRC2. In addition, the final optimized components will be tested either in wind tunnel or in flight in the framework of GRC2, in order to verify the predicted margins of improvement.

The expected impacts can be seen as twofold: the first is product-specific, therefore "technical" and the second is more general and we shall refer to it as “social". In fact, both can have a deeper influence on the European competitiveness.

From the technical point of view, the development of a multi-objective optimization platform will have a positive impact on the reduction of the time-to-market for helicopter and aircraft industries, which will be able to develop aircraft components faster, better and cheaper, as per a reduction in the wind tunnel costs which will decrease the industrial development costs. Moreover, when optimized components will be implemented and industrialized, this will lead to more efficient vehicles having a reduced drag, which will have also a positive impact on the fuel consumption, an aspect which can be seen in direct connection to the "eco-design" concept. Referring to helicopter, a step toward a wider diffusion of such kind of aircrafts is foreseen with the help of the present work. Actually, the development of more efficient and affordable helicopters is seen as one of the strategic plans for a decongestion in the air traffic.

All the participants in the Green Rotorcraft Consortium will benefit from HEAVYcOPTer, as the compiled version of the optimization toolbox will be available to each partner. The generality of the approach implemented will make it possible for aircraft industries to use the toolbox according to the specific objective functions of interest. In fact, the provision of best optimization approaches directly strengthens the competitiveness of the European aircraft industry, which is in alignment with the objectives of THEME 7 "Transportation" of the FP7.

Regarding the "social" impact, a much wider view is envisaged. The alignment of the proposal objectives is directly in accordance with “greener” pan-European transport systems for the benefit of all citizens and society and climate policy, which are declared as main drivers of the THEME 7 according to the actual work program.

Moreover, a social impact in terms of improved knowledge is expected: specifically, due to the academic nature of one of the participants, one major dissemination opportunity was given by publications. In particular, a series of scientific and promotional papers, web sites, seminars and University lessons have been carried out during the project and will be implemented after the project closure as well. The HEAVYcOPTer project has potential innovation impacts on the actual state of the art: both scientific journals and international conferences have been used to explain the novelties and the wide applicability of the proposed research, even in a non-aeronautical field. At the same time, this publication activity, especially conferences, has been a way of exploitation, in that other helicopter or fixed-wing aircraft manufacturers could take advantage of the adopted approach and use it directly or derive analogous methodologies.

Moreover, the project achievements and knowledge have been transferred to the education of the new generation of aerospace engineers. This has enabled students to actively participate in upstream research activities and has given them the opportunity to perform applied research in cooperation with the elite of the European aeronautics industry. In addition, this has had a positive impact on recruitment of young PhD students and researchers involved in the development of advanced design methodologies for more efficient helicopter and aerial vehicles. Finally, a special effort has been made to support young scientists and engineers for their training and in order to attract their interest in the topic and in flight physics in general, by holding workshops with external scientists and students.

The dissemination strategy has been intended to optimize dissemination of project knowledge to organizations that may be interested in the technological results and in the further development and/or applications of the main project achievements. To this purpose, favorable conditions will be created to facilitate exploitation even after the end of project. Specifically, with the project completion, the following main outputs are made available for further exploitation:

- Best practice approach for reliable helicopter engine installation simulations using advanced numerical high-fidelity tools;
- Advanced high-fidelity, multi-objective optimization procedures for enhancing helicopter efficiency;
- Fundamental knowledge on the design process of the engine installation system components;
- Final assessment of the overall engine installation performance.

As already mentioned, one of the proposal main strengths was that the whole optimization chain was released to the GRC Consortium at the end of the Project, following the typical rules of open source software, thus allowing end-users to access and exploit the developed tool in their research or work for free. This approach ensures that the beneficiary of the EC funding will not be limited solely to the leading industry, but the whole GRC Consortium will be able to exploit its achievements.
The delivered optimization chain includes the optimization platform in a compiled version, i.e. the GeDEA optimizer, all the interfaces with Hypermesh®, TGrid® and Fluent®, along with the pertinent theoretical and user's guides as well as a tutorial on how to use it.
Since the Topic is targeted at improving efficiency of aircraft components, the user groups of the results may consist mainly of the industrial companies and research institutions of this sector. Through the final assessment phase of the project, an effective design process and the potential of multi-objective aerodynamic optimization can be exploited by GRC Consortium partners. This ensures the dissemination and exploitation of the achievements to the European aircraft industry and research community.

**Provide the public website address (if applicable), as well as relevant contact details.**

N/A